Climate Dynamics (2019) 53:5165–5186
https://doi.org/10.1007/s00382-019-04844-8

ORIGINAL ARTICLE

Observed structural relationships between ocean chlorophyll variability and its heating effects on the ENSO

Rong-Hua Zhang[1,2,3,4,5] · **Feng Tian**[1,2,5] · **Hai Zhi**[6] · **Xianbiao Kang**[7]

Received: 10 January 2019 / Accepted: 4 June 2019 / Published online: 11 June 2019

Abstract

Ocean chlorophyll (Chl)-induced heating can affect the climate system through the penetration of solar radiation in the upper ocean. Currently, the ocean biology-induced heating (OBH) feedback effects on the climate in the tropical Pacific are still not well understood, and the mechanisms regarding how SST is modulated remain elusive. In this paper, chlorophyll (Chl) data from satellites are combined with physical fields from Argo profiles to estimate OBH-related fields, including the penetration depth (H_p) and the ocean mixed-layer (ML) depth (H_m). In addition, some directly related heating terms with H_m and H_p are diagnosed, including the absorbed solar radiation component within the ML (denoted as Q_{abs}), the rate of ML temperature changes that are directly induced by Q_{abs} (denoted as $R_{sr}=Q_{abs}/(\rho_0 C_p H_m)$), and the portion of solar radiation that penetrates through the bottom of the ML (denoted as Q_{pen}). The structural relationships between these related fields are examined to illustrate how these heating terms are affected by H_p and H_m. The extent to which R_{sr} and Q_{pen} are modulated by H_p is strikingly different during ENSO cycles. In the western-central equatorial Pacific, inter-annual variations in H_p tend to be out of phase with those in H_m. A decrease (increase) in Q_{abs} from a positive (negative) H_p anomaly during El Niño (La Niña) tends to be offset by a negative (positive) H_m anomaly. Thus, R_{sr} is not closely related with H_p, even though Q_{abs} is highly correlated with H_p, indicating that the direct thermal effect through Q_{abs} is not a dominant factor that affects the SST. In contrast, the inter-annual variability of Q_{pen} in the region is significantly enhanced by that of H_p, with their high positive correlation. The H_p-induced differential heating in the ML and subsurface layers from the Q_{pen} and Q_{abs} terms modifies the thermal contrast, stratification and vertical mixing, which represent a dominant indirect ocean dynamical effect on the SST. The revealed relationships between these related fields provide an observational basis for gaining structural insights into the OBH feedback effects and validating model simulations in the tropical Pacific.

Keywords Chlorophyll variability · Ocean biology-induced heating · ENSO modulations · The penetration depth and mixed layer depth · Satellite and Argo data

1 Introduction

Interactions between multiple processes are prominent in the tropical Pacific and are responsible for seasonal and inter-annual variabilities. For example, ocean–atmosphere coupling in the region creates the El Niño Southern Oscillation (ENSO), which is a dominant inter-annual mode in the climate system (e.g. Philander 1983; Zebiak and Cane 1987; Zhang and Levitus 1997; Zhang and Gao 2016; Tang et al. 2018). Additionally, various feedbacks and couplings

✉ Rong-Hua Zhang
rzhang@qdio.ac.cn

1 CAS Key Laboratory of Ocean Circulation and Waves, Institute of Oceanology, Chinese Academy of Sciences, Qingdao 266071, China

2 Center for Ocean Mega-Science, Chinese Academy of Sciences, Qingdao 266071, China

3 Center for Excellence in Quaternary Science and Global Change, Chinese Academy of Sciences, Xi'an 710061, China

4 Qingdao National Laboratory for Marine Science and Technology, Qingdao 266237, China

5 University of Chinese Academy of Sciences, Beijing 10029, China

6 College of Atmospheric Sciences, Nanjing University of Information Science and Technology, Nanjing 210044, China

7 College of Air Traffic Management, Civil Aviation Flight University of China, Guanghan 618307, China

coexist in the tropical Pacific that involve interactions among ocean physics, ocean biology and the climate, which can significantly modulate the ENSO (Zhang and Busalacchi 2008, 2009; Zhang et al. 2012; Zhi et al. 2015; Kang et al. 2017a, b). In particular, ocean biology can influence ocean physics through its modulation of penetrative solar radiation in the upper ocean (Timmermann and Jin 2002; Marzeion et al. 2005; Wetzel et al. 2006; Lengaigne et al. 2007; Gnanadesikan and Anderson 2009; Zhang et al. 2009; Anderson et al. 2009; Jochum et al. 2010; Park et al. 2014). Indeed, recent studies revealed pronounced ocean biology-induced heating feedback on the ENSO over the tropical Pacific (Zhang 2015; Kang et al. 2017a). As a major driver that strongly affects the upwelling and mixing processes in the equatorial Pacific, the ENSO greatly changes the Chl in the region. At the same time, corresponding biological perturbations modulate the penetrative solar radiation in the upper ocean, which produces a feedback on the ENSO.

The solar radiation that arrives at the sea surface penetrates through the upper water column and its shortwave component decays exponentially with depth. Some is absorbed directly within the mixed layer (ML), while some penetrates through the bottom of the ML and into subsurface layers. The ML depth (H_m) is a major physical factor that determines the vertical partitioning of solar radiation between the mixed layer (ML) and subsurface layers. Additionally, phytoplankton, detritus and colored dissolved organic matter (CDOM) can absorb solar radiation mainly in the visible spectrum (380–700 nm), thus affecting the vertical penetration of the incoming solar radiation in the upper ocean (Lewis et al. 1990; Morel and Antoine 1994; Siegel et al. 2002; Strutton and Chavez 2004; Kang et al. 2017a). Among these components, chlorophyll is the main factor that attenuates shortwave radiation and consequently affects the ocean's thermal conditions. Correspondingly, a penetration depth (H_p) can be defined to represent the extent to which the penetration of solar radiation in the upper ocean is affected by the Chl concentration. Thus, the depth of the mixed layer (H_m) and penetration depth (H_p) are two factors that affect the distribution of penetrative solar radiation in the ML and subsurface layers; the former (H_m) is controlled by physical processes and the latter (H_p) is determined by biological processes. Furthermore, bio-effects are realized through a few heating terms that are directly associated with Chl (and the corresponding H_p) and H_m, including the absorbed solar radiation flux within the ML (denoted as Q_{abs}) and its directly related temporal rate of change in the ML temperature (denoted as R_{sr}), alongside the penetrated portion of solar radiation through the bottom of the ML (denoted as Q_{pen}). These heating terms can be used to characterize and quantify the Chl-induced heating feedback effects on the SST because these terms act to modulate the thermodynamics in the upper ocean, which can further induce indirect dynamical effects on the SST.

Previously, bio-climate interactions were investigated by using coupled ocean–atmosphere models with different degrees of complexity. Large uncertainties exist in model representations of ocean biology-induced heating (OBH) feedback, and its simulated effects strongly depend on models used. Thus, modulations in SST from ocean biology are sensitive to the manner in which bio-effects are represented in models. Currently, models exhibit biases in terms of simulating Chl variability in the tropical Pacific. Additionally, the physical mechanisms that are involved in bio-effects significantly differ among various previous modeling studies because different dominant processes are apparently at work. What are the main factors that control ocean biology-induced effects and the involved physical processes? Why do large intermodal differences exist in bio-effect simulations? Clearly, observations are vital to reveal the physical mechanism for these ocean biology-induced effects and validate model-based simulations and related bio-effects.

Over the past decade, remote sensing has made great progress in providing time series of ocean color data and associated products. For example, chlorophyll (Chl) data are available from satellite measurements and have been used to describe and understand bio-climate interactions (McClain et al. 1998). As observed in the tropical Pacific, for example, the existence and variations of Chl affect surface-layer water turbidity and modify the vertical redistribution of solar radiation in the upper ocean. Correspondingly, the Chl concentration can be used to estimate H_p. Also, Argo profiles provide unprecedented temperature and salinity data in the upper ocean, which can be used to estimate ocean fields on basin scales, including the depth of the ML (H_m). Thus, sufficient observational data of Chl and physical fields have been accumulated in the last decade, which allows us to perform detailed analyses on Chl-induced heating effects in the tropical Pacific.

In this paper, we perform an observation-based analysis for the biological heating effect, with a focus on the inter-annual variability that is associated with the ENSO in the tropical Pacific. A diagnostic analysis method is developed that makes full use of observational data to reveal bio-effects from inter-annual Chl anomalies. More specifically, observed Chl data are combined with other derived fields to characterize the structural relationships of Chl-related heating terms with H_m and H_p. For example, observed H_m and H_p fields are used to quantify the combined effects on the penetration of solar radiation and related heating effects. The revealed relationships are used to infer the processes that are involved and understand the influence pathways through which the SST is modulated by inter-annual Chl anomalies.

This paper is organized as follows. Section 2 describes the heating terms that are associated with Chl and the observational data that are used for the analyses. The structural relationships of these heating terms with H_m and H_p are analyzed in Sect. 3. Section 4 provides a summary and discussion. An Appendix is provided for the analyses of the annual mean and seasonal variations in some related fields.

2 Ocean Chl-induced heating terms and observational data

Comprehensive data are used to diagnose Chl-induced heating terms and bio-effects on the SST, including ocean physical and biological fields that are derived from satellite-based observations and in situ Argo profiles. As shown below, these heating terms are determined by the ocean mixed-layer depth (H_m) and penetration depth (H_p); the former is determined by physical processes and the latter is determined by biological processes. Observational data are used to quantify these heating terms and structural relationships between physical and biological fields. The effects on these terms can be analyzed using observational data, which are defined below.

2.1 Ocean Chl-induced heating terms

The incoming solar radiation that arrives at the sea surface tends to decay very sharply with depth in the upper ocean (a factor that reflects the effect of pure water on penetrative solar radiation); the depth of the mixed layer (H_m) is a major factor that determines the vertical partitioning of solar radiation between the mixed layer (ML) and subsurface layers. At the same time, the existence and variations of Chl can affect the penetrative solar radiation in the upper ocean; therefore, the penetration depth (H_p) can be introduced to quantify the extent to which solar radiation is affected by biological fields in the upper ocean.

Some heating-term fields are directly related to H_p and H_m, including the absorbed solar radiation flux within the ML (denoted as Q_{abs}) and its directly related temporal rate of change in the ML temperature (denoted as R_{sr}), alongside the portion of solar radiation that penetrates the bottom of the ML (denoted as Q_{pen}).

2.1.1 Penetration depth (H_p)

Ocean biological components (such as phytoplankton, detritus and colored dissolved organic matter (CDOM)) can absorb solar radiation in the visible spectrum (380–700 nm) and further modify the vertical penetration of the incoming solar radiation in the upper ocean (Lewis et al. 1990; Morel and Antoine 1994; Siegel et al. 2002; Strutton and Chavez 2004). The penetration of the solar shortwave radiation in the upper ocean follows the Beer-Lambert Law, which indicates that shortwave radiation decays exponentially with depth according to attenuation coefficients. Here, chlorophyll is considered to have attenuating effects on shortwave radiation.

Thus, the total attenuation coefficient can be computed as follows (Wang et al. 2008):

$$K_A(z) = K_W + K_C Chl(z), \tag{1}$$

where z is the depth; $K_W = 0.028\ m^{-1}$ and $K_C = 0.058\ m^{-1}$ (mg chl m^{-3})$^{-1}$ represent the attenuation coefficients for pure water and chlorophyll, respectively; and Chl(z) is the chlorophyll concentration. In this study, we only consider the Chl effect on K_A because Chl plays a dominant role in ocean biology-induced heating effects.

Then, a penetration depth (H_p) of the shortwave radiation is defined as the inverse of K_A calculated from the satellite observations of the Chl field (Murtugudde et al. 2002; Zhang et al. 2011). This H_p field serves as a linkage between ocean biology and physics and can be used to quantify the ocean biology-induced heating effects on the related heating terms.

2.1.2 Absorbed solar radiation within the ML (Q_{abs} and R_{sr})

As expressed in Zhang (2015), H_p and H_m are explicitly associated with several ocean biology-induced heating terms. Q_{abs} denotes the absorbed solar radiation flux within the ML, and R_{sr} denotes the temporal rate of change in the ML temperature that directly results from the Q_{abs} effect on SST, both of which are written as follows

$$Q_{abs}(H_m, H_p) = Q_{sr}[1 - \gamma \exp(-H_m/H_p)], \tag{2}$$

$$R_{sr}(H_m, H_p) = Q_{sr}[1 - \gamma \exp(-H_m/H_p)]/(\rho_0 c_p H_m) = Q_{abs}/(\rho_0 c_p H_m), \tag{3}$$

where Q_{sr} is the incoming solar radiation flux at the sea surface, γ is a constant (=0.33) that denotes the fraction of the available radiation to penetrate to depths beyond the first few centimeters of the sea surface, C_p is the heat capacity, and ρ_0 is the density of sea water.

As expressed above, Q_{abs}, which is a function of both H_m and H_p, is determined by changes in H_m and H_p. On the one hand, Q_{abs} increases exponentially with H_m. The deeper the ML, the more solar radiation that is directly absorbed within the ML. On the other hand, Q_{abs} also decreases exponentially with H_p; the larger the H_p value, the less solar radiation that is directly absorbed within the ML, producing more penetration through the bottom of the ML. Therefore, changes in H_m and H_p tend to have an opposite effect on Q_{abs}. That is, a negative (positive) perturbation in H_m reduces (increases) Q_{abs}, whereas a negative (positive) perturbation in H_p increases (reduces) Q_{abs}.

Furthermore, the absorbed solar radiation within the ML (Q_{abs}) directly changes R_{sr}, thus further changing the

SST, which represents a direct thermal effect. R_{sr} is proportional to Q_{abs} (which has an exponential relationship with H_m and H_p) and inversely proportional to H_m (appearing as a denominator). Thus, R_{sr} can be affected by H_m in two fashions, whose effects tend to be of opposite signs. On the one hand, H_m is exponentially related to Q_{abs}, so a deepening (shoaling) of the ML (which increases (decreases) Q_{abs}) can increase (decrease) R_{sr}. On the other hand, H_m is inversely proportional to R_{sr} (appearing as a denominator), so the deepening (shoaling) of the ML can decrease (increase) R_{sr}. These two effects on R_{sr} that are induced by H_m and H_p have implications for how this term is modulated by H_p.

2.1.3 Penetrative solar radiation flux through the bottom of the ML (Q_{pen})

The solar radiation flux that penetrates the bottom of the ML (Q_{pen}) is written as

$$Q_{pen}(H_m, H_p) = Q_{sr}[\gamma \exp(-H_m/H_p)] = Q_{sr} - Q_{abs}. \quad (4)$$

As expressed, Q_{pen} has exponential relationships with H_m and H_p, which tend to have opposite signs relative to Q_{abs}. For example, Q_{pen} decreases exponentially with H_m but increases exponentially with H_p; that is, the deeper the ML, the less solar radiation that directly penetrates through the bottom of the ML. Similarly, the larger the H_p value, the deeper that the solar radiation directly penetrates into the subsurface layer. Therefore, changes in H_m and H_p tend to have opposite effects on Q_{pen}.

2.2 Observational data

Various observational data are used to describe the inter-annual variability and relationships among some physical and biological fields. The SST fields are obtained from Reynolds et al. (2002). The shortwave solar radiation data are from the MERRA re-analysis product (Rienecker et al. 2011). The surface chlorophyll datasets are obtained from the GlobColour project from 1998 to 2007, which supplied continuous datasets for merged Level-3 Ocean Color products (including the SeaWIFS, MODIS, MERIS and VIIRS sensors; see details at http://hermes.acri.fr/index.php; Maritorena et al. 2010). Then, monthly CHL-1 data (chlorophyll concentration (mgm^{-3}) for case-1 waters) are interpolated from $0.25° \times 0.25°$ grids to our analysis grids ($1.0° \times 1.0°$).

The Argo-based dataset is provided by the International Pacific Research Center (IPRC)/Asia–Pacific Data-Research Center (APDRC). This product includes the MLD and three-dimensional gridded fields for temperature and salinity with a 1° horizontal resolution at the standard depths. The MLD is defined as the depth at which the density increases from 10 m to a value that is equivalent to a temperature drop of 0.2 °C.

These data during 2005–2015 are averaged to form climatological monthly fields, which are used to calculate their inter-annual anomalies. In addition to these directly observed data, some related heating fields are estimated, including a penetration depth (H_p), Q_{abs}, R_{sr}, and Q_{pen}.

3 Structural relationships associated with the bio-effects on ENSO

Figures 1, 2, and 3 display the evolution along the Equator for various related total fields; the corresponding annual-mean and seasonal variations are presented in the Appendix. The inter-annual variabilities of these physical and biological fields are dominated by ENSO signals in the tropical Pacific. Note that full quantity and its variability exhibit differences in their magnitudes between physical and biological fields. For example, seasonal and inter-annual variabilities of physical fields are generally one order of magnitude smaller than its total field. However, the magnitudes of seasonal and inter-annual Chl variabilities are comparable to those of its total value, and the total Q_{abs} field is one order of magnitude larger than its seasonal and inter-annual variability.

3.1 Inter-annual variations in SST and Chl

The total SST field (Fig. 1a) is characterized by a warm pool in the western tropical Pacific and a cold tongue in the eastern equatorial Pacific. The warm pool in the west and cold tongue in the east exhibit large zonal displacements during ENSO cycles. During La Niña, the warm pool retreats to the west, whereas the cold tongue in the east develops and expands westward along the Equator, with the 25 °C SST isotherm located west of 150°W. During El Niño, the warm waters in the west extend eastward along the Equator (e.g., the 27 °C SST isotherm extends eastward to the east of 150°W), while the cold tongue shrinks in the east.

As a major driver, the ENSO induces pronounced perturbations to ocean physical and biological fields in the tropical Pacific (Figs. 1, 2). For example, shortwave radiation exhibited a pronounced inter-annual variation associated with ENSO (Fig. 2a); one interesting feature is the large shift for shortwave radiation around 2010. We speculate that the eastward migration of atmospheric convection center during El Niño is responsible for a decrease in shortwave radiation near the dateline. During 2009-2010, a record-breaking warm sea surface temperature emerged in the central Pacific, which is the strongest Central Pacific type of El Niño in the 21th century (Lee and McPhaden 2010). In terms of biological field, a well-defined pattern of inter-annual Chl variability is seen during El Niño and La Niña cycles. The main characteristics of the mean Chl field and variability have been previously described (e.g. Ballabrera-Poy et al.

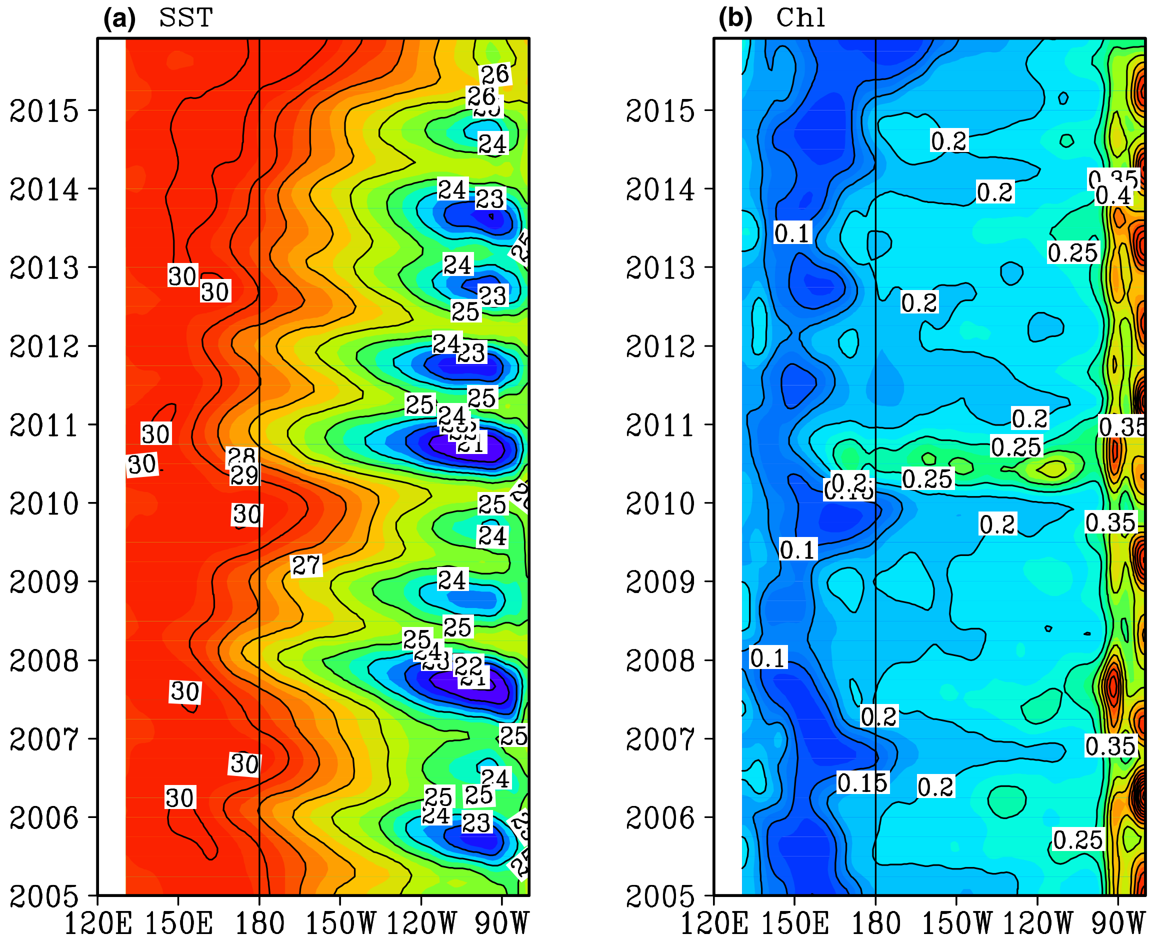

Fig. 1 Time-longitude sections along the Equator during 2005–2015 for the **a** SST and **b** Chl fields from the GlobColour Project. The contour interval is 1 °C in **a** and 0.05 mg m^{-3} in **b**

2007). Climatologically (see Fig. 1b and the Appendix), Chl exhibits elevated values from the west to the east across the tropical Pacific: its concentration is low (< 0.1 mg m^{-3}) in the western equatorial Pacific in association with the warm waters but is high (> 0.2 mg m^{-3}) in the eastern equatorial region, where the cold tongue develops. Additionally, the Chl concentration is very high in the eastern coastal regions.

Inter-annually, the Chl concentration in the equatorial Pacific significant increases during La Niña events and drops during El Niño events. Detailed examinations indicate that the inter-annual Chl variability exhibits different characteristics in the west and east. In the western-central equatorial Pacific, the Chl field has a clear east–west migration along the Equator during ENSO cycles. Regions with large values extend to the date line during El Niño. In the eastern equatorial Pacific, large variations are associated with local oceanic processes (e.g., upwelling).

The inter-annual variability features of the SST and Chl fields can be more clearly seen in their anomaly fields (Fig. 4). The magnitude of the inter-annual Chl variability is comparable to that of the total Chl field. ENSO is a major source for inter-annual variability of Chl, with negative anomaly during El Niño events and positive anomaly during La Niña events. The inter-annual Chl variations in the east do not exhibit obvious propagation along the Equator (i.e., they are almost in phase in terms of time), but those in the west have zonal migration along the Equator (Fig. 1). The inter-annual Chl variability is quantified by calculating its standard deviations (Fig. 5a). Two large Chl variability centers are seen: one in the western equatorial Pacific to the west of the date line and another in the eastern equatorial and coastal regions.

Clear relationships exist between the inter-annual variations in SST and Chl; the latter closely follows the former, characterized by their out-of-phase fluctuations during ENSO cycles (Fig. 4). Thus, the ENSO induces bio-responses that are quick and coherent at large scales. In addition, the Chl and SST exhibit spatial shifts in their large variability regions. While the largest SST anomalies occur in the central and eastern equatorial Pacific (Fig. 4a),

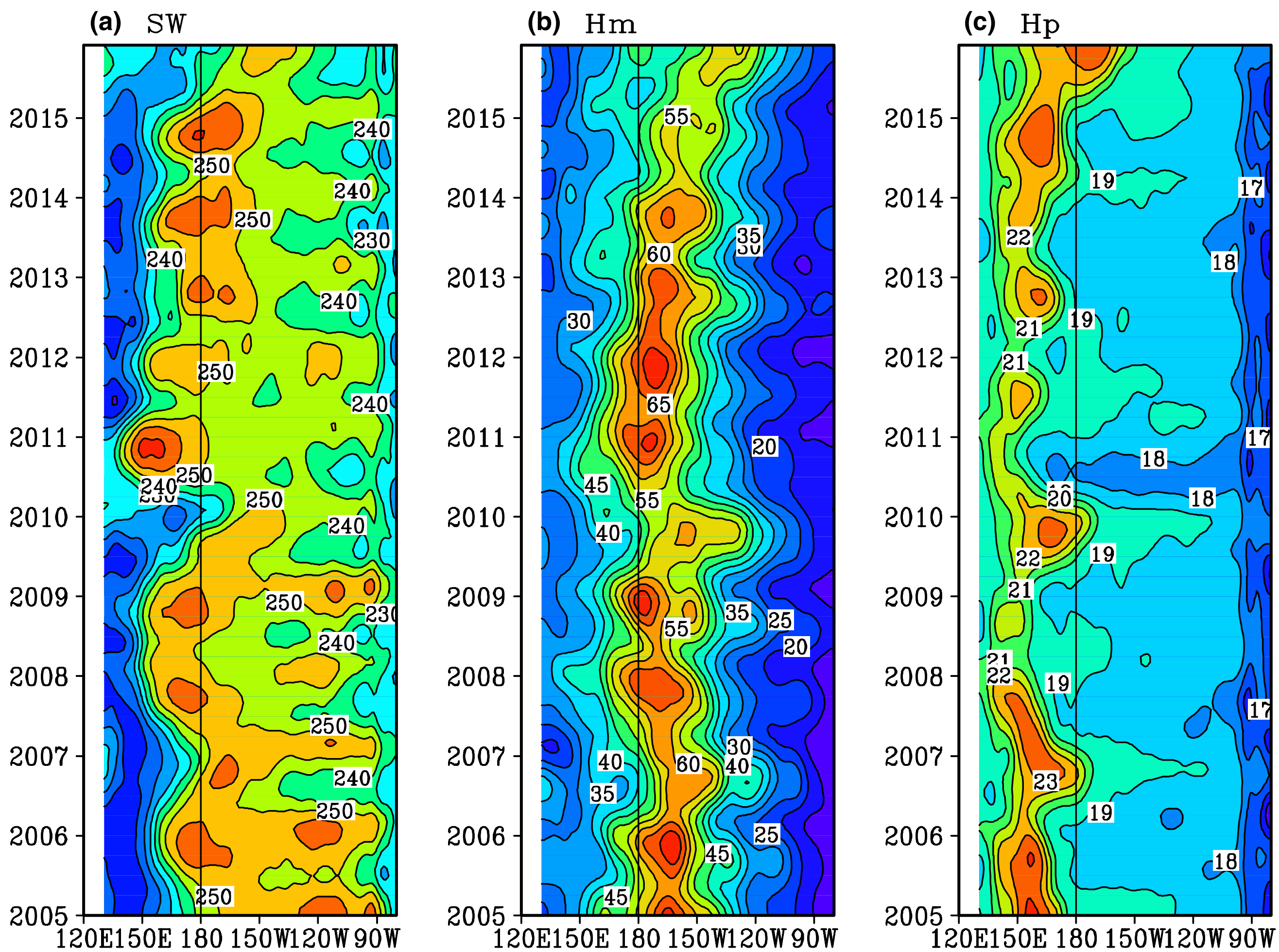

Fig. 2 Time-longitude sections along the Equator during 2005–2015 for the **a** shortwave radiation, **b** H_m, and **c** H_p fields. The contour interval is 10 W m^{-2} in **a**, 5 m in **b**, and 1 m in **c**

a pronounced inter-annual variability of Chl is located in the western-central equatorial Pacific (Fig. 4b). During La Niña events, for example, a cold SST anomaly is located in the central-eastern equatorial Pacific, but regions with positive Chl concentration are seen in the western-central equatorial region. In contrast, during El Niño events, a warm SST anomaly in the east is associated with a negative Chl concentration in the west. Quantitatively, the correlations between SST and Chl are shown in Fig. 6a. The inter-annual variability of Chl closely follows that of SST, so the inter-annual variations in Chl tend to be negatively correlated with those in the SST over the tropical Pacific, with large negative values in the western equatorial Pacific near the date line.

3.2 Inter-annual variations in H_m and H_p

The characteristics of the H_m structure and its variability are seen in Fig. 2b and the Appendix. The ML is relatively shallow (< 30 m) in the western tropical Pacific because of the weak surface friction velocity and stabilizing surface buoyancy flux. Regions with values larger than 50 m are found in the central basin, which exhibit energetic surface wind and strong surface buoyancy losses. During La Niña, the ML is unusually deep in the western-central equatorial Pacific but shallow in the eastern regions. During El Niño, the ML becomes shallower in the west but deeper in the east. The inter-annual variations in H_m exhibit a see-saw pattern, with two large anomaly regions in the western and eastern equatorial regions (Fig. 7b) and the zero-crossing line around 150°W. As such, inter-annual anomalies of H_m in the west tend to be out of phase with those in the east, a clear see-saw pattern that is associated with the ENSO's evolution.

The above Chl field is used to estimate the penetration depth (H_p). As shown in Fig. 2c and the Appendix, the penetration of solar radiation is deep in the western equatorial Pacific but shallow in the east, with a low H_p value (< 19 m) in the east and high H_p value (> 20 m) in the west. Seasonally

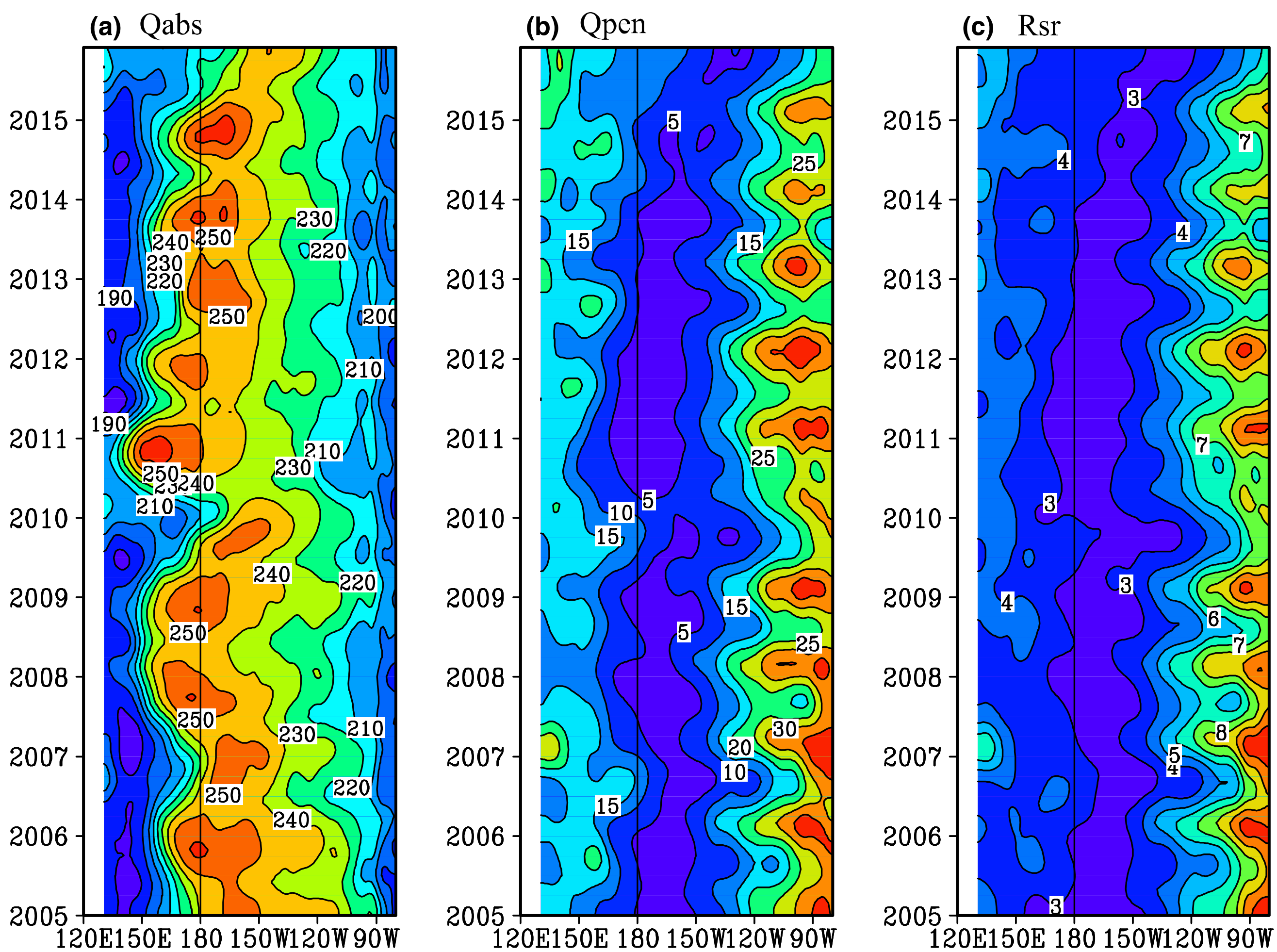

Fig. 3 Time-longitude sections along the Equator during 2005–2015 for the ocean Chl-related total heating terms: **a** Q_{abs}, **b** Q_{pen}, and **c** R_{sr}. The contour interval is 10 W m^{-2} in **a**, 5 W m^{-2} in **b** and 1 °C $month^{-1}$ in **c**

(see the Appendix), the penetration of solar radiation is deep in spring but shallow in fall. Inter-annually, the penetration depth in the equatorial Pacific exhibits large variations during ENSO cycles (Fig. 7c). Inter-annual H_p anomalies have a uniform pattern across the equatorial Pacific. For example, H_p has positive anomalies in the equatorial Pacific during El Niño (corresponding to a reduced Chl concentration with a deeper penetration of solar radiation) but negative anomalies during La Niña (corresponding to an increased Chl concentration with a shallower penetration of solar radiation).

As a response to ENSO cycles, the inter-annual variations in H_m and H_p indicate a coherent space–time structure (Figs. 7b, c, 8, 9) clearly display their horizontal patterns during La Niña conditions as represented in August 2010 and during El Niño conditions in August 2015, respectively. One striking feature is that the inter-annual variations in H_p and H_m tend to be out of phase in the western-central equatorial Pacific during ENSO cycles but in phase in the east (Figs. 8b, c, 9b, c). That is, in the western equatorial Pacific, positive (negative) H_m anomalies are accompanied by negative (positive) H_p anomalies during La Niña (El Niño). However, in the eastern equatorial Pacific, H_p anomalies are weak and H_m has positive and negative anomalies during El Niño and La Niña, respectively.

The standard deviations for the inter-annual anomalies of H_p and H_m are shown in Fig. 5b, c. Regions with large inter-annual H_p variability are seen in the western Pacific west of the date line. H_m has a large-variability region in the western equatorial region. In the western-central equatorial Pacific near the date line, the magnitude of the inter-annual variability of H_p is approximately 20% that of H_m, indicating that the effect of H_p on the heating terms is not negligible compared to that of H_m. Quantitatively, the correlations between H_m and H_p are shown in Fig. 6c. Corresponding to the negative correlations between H_p and Chl, positive correlations exist between H_p and H_m in the western equatorial Pacific. The regions with large positive correlation near the date line are consistent with those where the amplitude of H_p

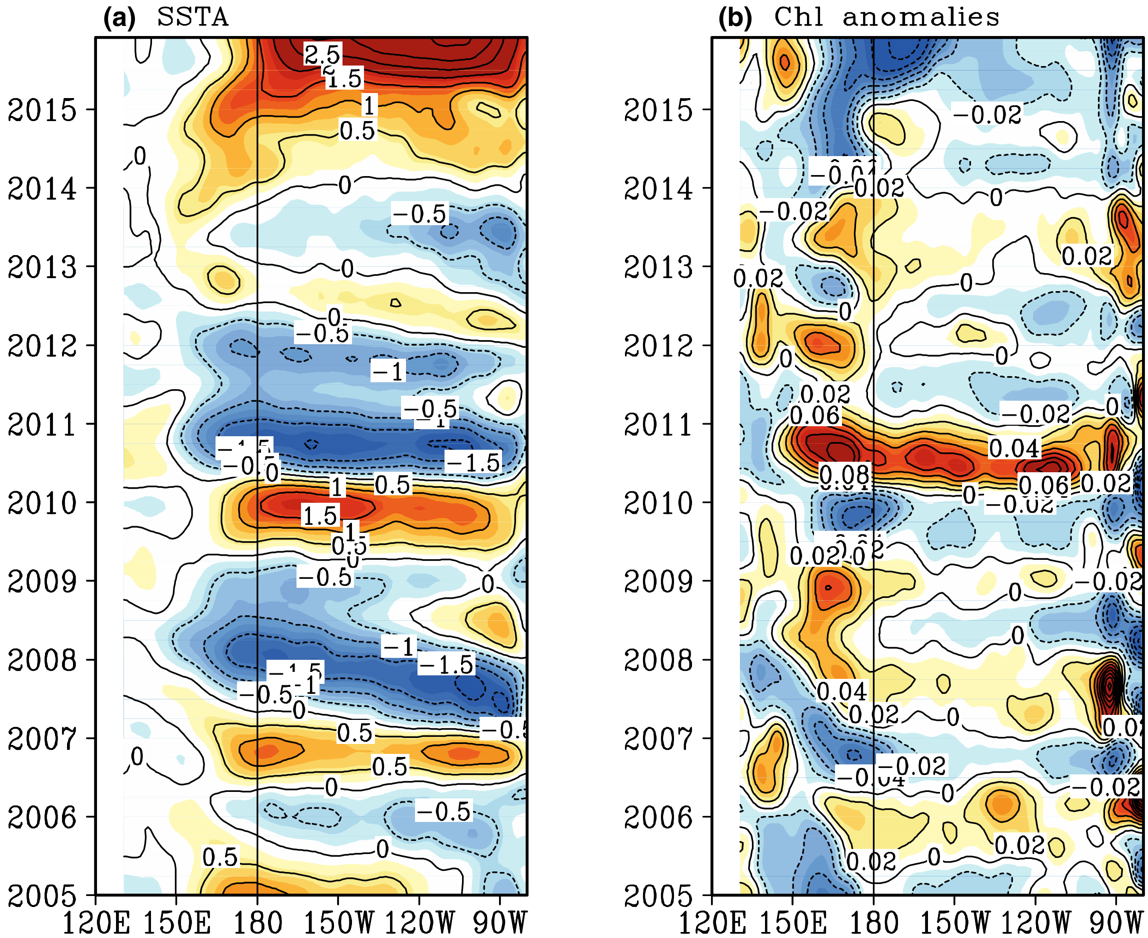

Fig. 4 Time-longitude sections along the Equator during 2005–2015 for inter-annual anomalies of **a** SST and **b** Chl. The contour interval is 0.5 °C in **a** and 0.02 mg m^{-3} in **b**

is approximately 20% that of H_m, indicating that H_p can have pronounced effects. The effects on the heating terms from the inter-annual variability of H_p will be analyzed below.

3.3 Inter-annual variations in the bio-induced heating terms

H_m and H_p are two factors that determine the distribution of solar radiation between the mixed layer and underlying subsurface layers. As mathematically expressed above, the three heating terms are directly associated with H_m and H_p. To understand the bio-effects in the tropical Pacific, a diagnostic analysis is performed to quantify the structural relationships of these heating terms with H_m and H_p, with emphasis placed on the ENSO. Then, the manner in which these related fields are affected by H_p can be inferred to reveal how the SST is modulated by the bio-effects and underlying processes that are involved.

Figures 3, 10, 11, and 12 display the space–time evolution of some related fields along the Equator; examples for the horizontal patterns of inter-annual Q_{pen} anomalies are demonstrated in Fig. 8 during La Niña conditions and Fig. 9 El Niño conditions, respectively. All these fields exhibit large variability that is associated with the ENSO. The inter-annual variations in H_m and H_p exhibit well-defined structures during ENSO cycles, so their effects on the vertical distributions of solar radiation between the ML and subsurface layers are expected, which can be quantified by calculating the modulating effects on these heating terms. For example, the structural relationships of Q_{pen} with H_m and H_p can be clearly seen in the horizontal distributions of their inter-annual anomaly fields during El Niño (Fig. 8) and La Niña (Fig. 9), respectively.

As indicated in the H_m structure (Fig. 2b), most of the solar radiation is absorbed within the ML (Q_{abs}; Fig. 3a), with some penetrating through the bottom of the ML (Q_{pen}; Fig. 3b). When the ML changes during ENSO cycles, the amount of solar radiation that is absorbed within the ML (Q_{abs}) and penetrates through the bottom of the ML (Q_{pen}) also changes. The absorbed component within the ML

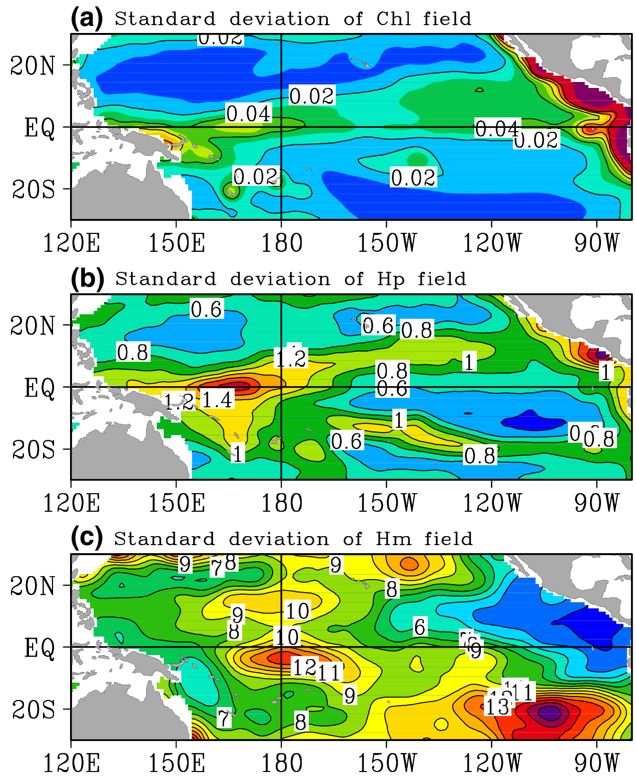

Fig. 5 Standard deviations for inter-annual anomalies of **a** Chl, **b** H_p and **c** H_m. The contour interval is 0.02 mg m^{-3} in **a**, 0.2 m in **b** and 1 m in **c**

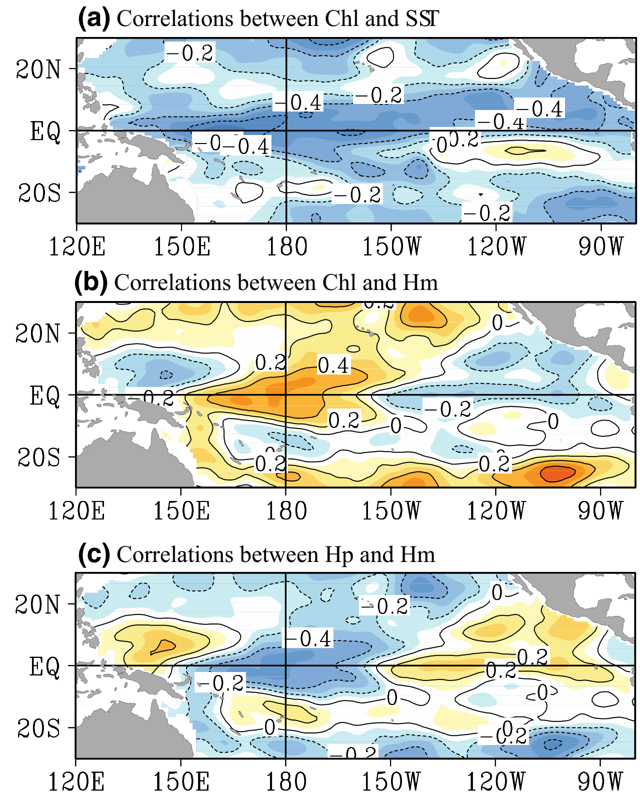

Fig. 6 Correlations during 2005–2015 between inter-annual anomalies of **a** Chl and SST, **b** Chl and H_m, and **c** H_p and H_m. The contour interval is 0.2

directly changes the R_{sr} value (Fig. 3c), thus modulating the SST, a way to directly change SST. Additionally, H_p can have a modulating effect on these terms, which is analyzed in detail below.

3.3.1 Modulating effect on Q_{pen}

The total Q_{pen} field and corresponding inter-annual Q_{pen} anomalies along the Equator (Figs. 3b, 10a) indicate their well-defined structure during ENSO cycles. Large Q_{pen} anomalies are observed in the equatorial regions with a see-saw pattern in the west and east, which is characterized by a positive Q_{pen} anomaly during El Niño and a negative anomaly during La Niña. In the east, an opposite pattern is seen during ENSO cycles.

Q_{pen} is affected by H_m and H_p (Fig. 3), and H_m's effect on Q_{pen} can be clearly seen in the horizontal distributions of the inter-annual anomaly fields during El Niño (Fig. 8) and La Niña (Fig. 9). In the western-central equatorial region, for example, the negative Q_{pen} anomaly during La Niña is accompanied by a positive H_m anomaly. An opposite pattern is seen during El Niño (Fig. 9), with a positive Q_{pen} anomaly accompanied by a negative H_m anomaly in the western-central region near the date line. The similarity between the space–time evolutions of H_m (Fig. 7b) and Q_{pen} (Fig. 10a) indicates that H_m is a main factor that determines the mean state and variations of Q_{pen} in the tropical Pacific.

Q_{pen} is also a function of H_p, so we expect that Q_{pen} can be modulated by H_p. As shown in Figs. 7c and 10a, negative and positive Q_{pen} anomalies have a clear signature of the inter-annual H_p effects. Thus, a close relationship exists between the inter-annual variations in H_p and Q_{pen} in the western-central equatorial basin. A negative H_p anomaly is observed during La Niña events, which causes less sunlight to penetrate through the bottom of the mixed layer, but become trapped more within the mixed layer. Thus, this negative H_p anomaly makes the negative Q_{pen} anomaly during La Niña *more negative*. During El Niño, when H_p becomes a positive anomaly, sunlight can penetrate deeper into subsurface layers, so the positive H_p anomaly makes the positive Q_{pen} anomaly *more positive*.

Clearly, the large observed inter-annual anomalies of Q_{pen} (e.g., Fig. 10a) represent a combined effect from both H_m and H_p during ENSO cycles. Although the inter-annual variability of Q_{pen} in this region is mainly determined by that of H_m, the inter-annual variability of H_p can also make a substantial contribution, enhancing inter-annual anomalies of Q_{pen} during El Niño-La Niña cycles.

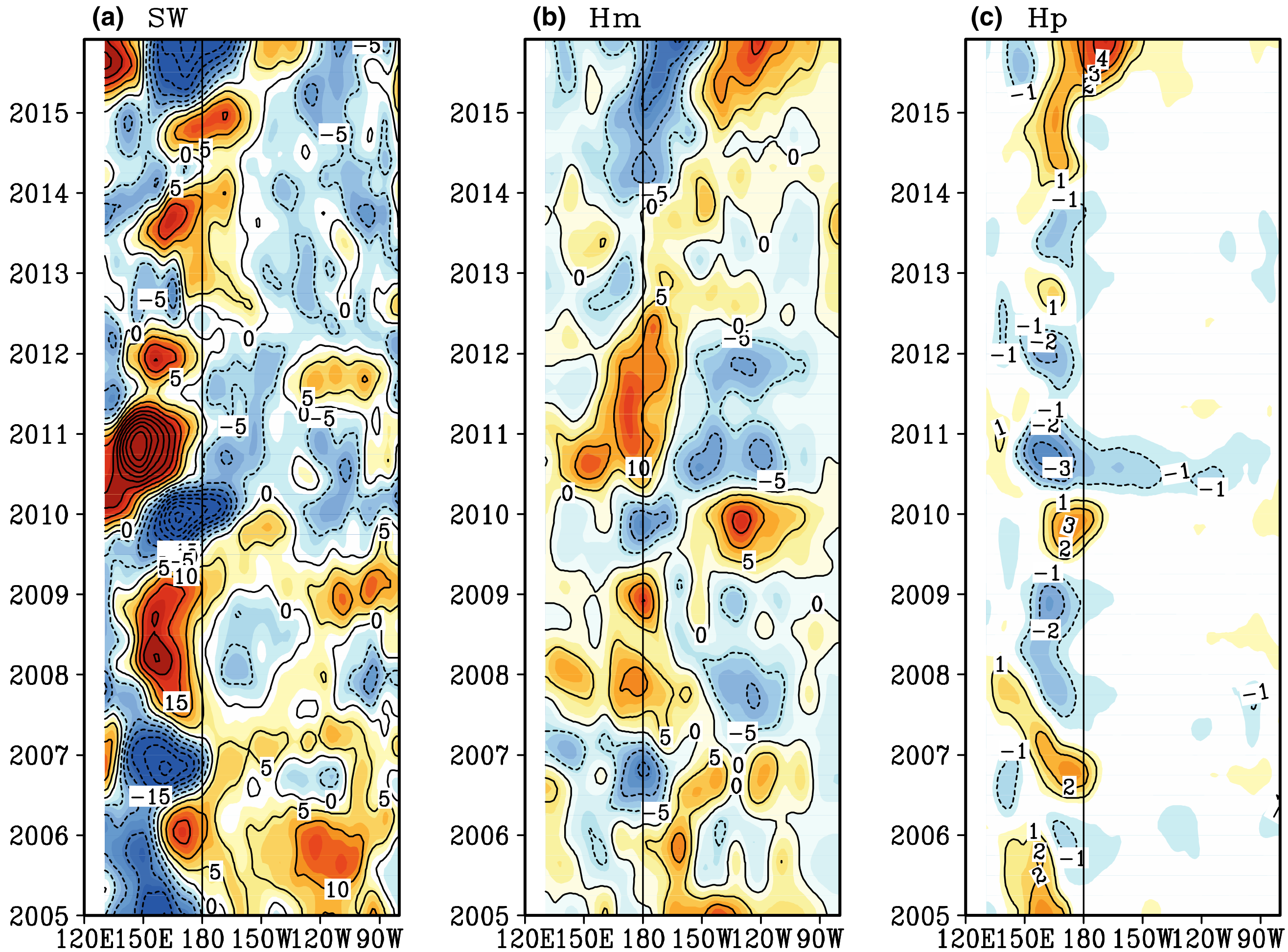

Fig. 7 Time-longitude sections along the Equator during 2005–2015 for inter-annual anomalies: **a** shortwave radiation, **b** H_m, and **c** H_p. The contour interval is 5 W m^{-2} in **a**, 5 m in **b**, and 1 m in **c**

3.3.2 Modulating effects on Q_{abs} and R_{sr}

Next, similar calculations are shown in Figs. 3a and 11 for Q_{abs}. Similar to Q_{pen}, the inter-annual variability in Q_{abs} exhibits a well-defined pattern during ENSO cycles. As defined above, the space–time structural relationships of Q_{abs}'s variability with H_m and H_p are similar to those of Q_{pen} but with the opposite sign. For example, in the western-central equatorial Pacific, Q_{abs} exhibits a positive anomaly during La Niña (more gain in solar radiation within the ML) but a negative anomaly during El Niño (loss of solar radiation within the ML), which is determined collectively by H_m and H_p. The inter-annual variability of Q_{abs} (Fig. 11a) almost mirrors that of H_m (Fig. 7b), so H_m is a major factor that controls the structure and variability of Q_{abs}. Additionally, Q_{abs} can be modulated by H_p because the former is a function of H_p. Similar to Q_{pen}, a change in H_p significantly modulates Q_{abs} in the western-central equatorial Pacific, and the observed inter-annual variability of Q_{abs} also represents the combined effects of H_m and H_p. During La Niña conditions, a positive H_m anomaly is mainly responsible for a positive Q_{abs} anomaly in the region; at the same time, H_p exhibits a negative anomaly, which increases the absorption of solar radiation within the ML (a corresponding positive Q_{abs} anomaly). Thus, the negative H_p anomaly makes the positive Q_{abs} anomaly *more positive*. The combined effects of the positive H_m anomaly and negative H_p anomaly enhance the positive Q_{abs} anomaly. During El Niño events, the negative H_m anomaly is responsible for a negative Q_{abs} anomaly in the western-central equatorial Pacific; then, the positive H_p anomaly makes the negative Q_{abs} anomaly *more negative*. Thus, the inter-annual variability of H_p tends to enhance inter-annual anomalies of Q_{abs} during ENSO cycles.

Next, we move to the analysis for R_{sr} (the rate of the ML temperature change that is directly resulted from the heating effect associated with Q_{abs}). Figures 3c and 12 display the total R_{sr} field and its inter-annual variability along the Equator. R_{sr} has high values in the west and east but relatively low

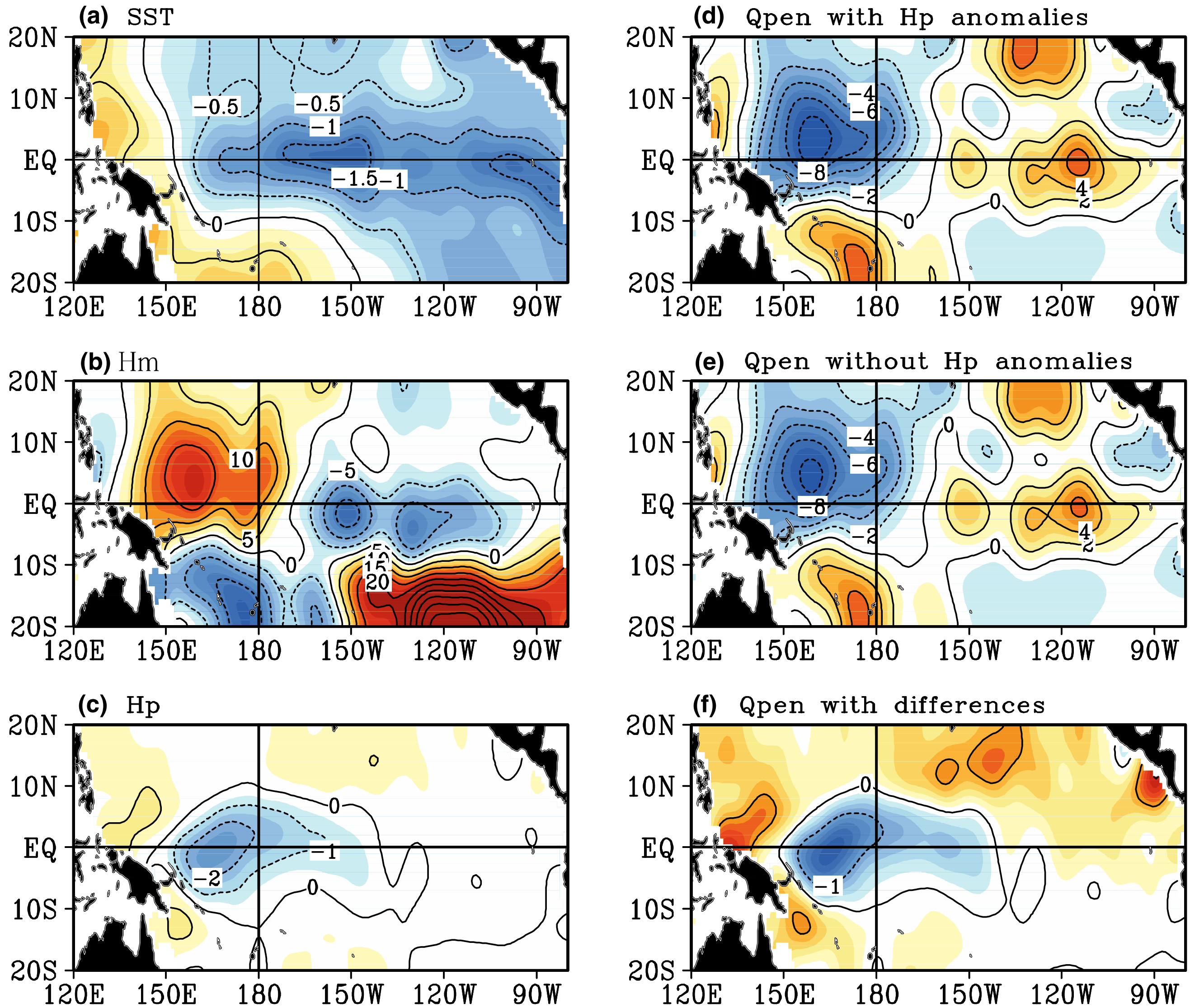

Fig. 8 Horizontal patterns of inter-annual anomaly fields for La Niña conditions as represented in August 2010: **a** SST, **b** H_m, **c** H_p, **d** Q_{pen} when estimated with the inter-annual H_p effect considered, **e** Q_{pen} when estimated with the inter-annual H_p effect excluded, and **f** the differences (the Q_{pen} fields estimated with the inter-annual H_p effect included minus those excluded). The contour interval is 0.5 °C in **a**, 5 m in **b**, 1 m in **c**, 2 W m^{-2} in **d** and **e**, and 1 W m^{-2} in **f**

values in the central basin (Fig. 3c and the Appendix). R_{sr} also exhibits large inter-annual variability that is associated with ENSO cycles. In the western-central equatorial regions, R_{sr} has a positive anomaly during El Niño events but a negative anomaly during La Niña events, which is determined by H_m and H_p. The inter-annual variability of R_{sr} (Fig. 12a) follows closely with that of H_m (Fig. 7b), so H_m is a major factor that determines the structure and variability of R_{sr}. R_{sr} is also a function of H_p, so we expect that R_{sr} can be modulated by H_p, as with Q_{abs} and Q_{pen}. However, the manner in which R_{sr} is affected by H_p is different from Q_{abs} and Q_{pen}, which is explained below.

As expressed by $R_{sr} = Q_{abs}/(\rho_0 C_p H_m)$, R_{sr} is determined by both Q_{abs} and H_m. On the one hand, Q_{abs}, which is a function of H_m and H_p, can be one factor that determines the R_{sr} value. That is, the absorbed solar radiation within the ML (Q_{abs}) directly affects the rate of the ML temperature change, so R_{sr} and Q_{abs} can have a coherent variation and can be modulated by H_p in a similar fashion. In the western-central region, for example, the positive H_p anomaly during El Niño decreases the absorption of solar radiation within the ML (a corresponding negative Q_{abs} anomaly), which would produce a negative R_{sr} anomaly with a negative correlation between H_p and R_{sr}. However, this scenario does not occur. Examining the relationship among the inter-annual variations in H_p

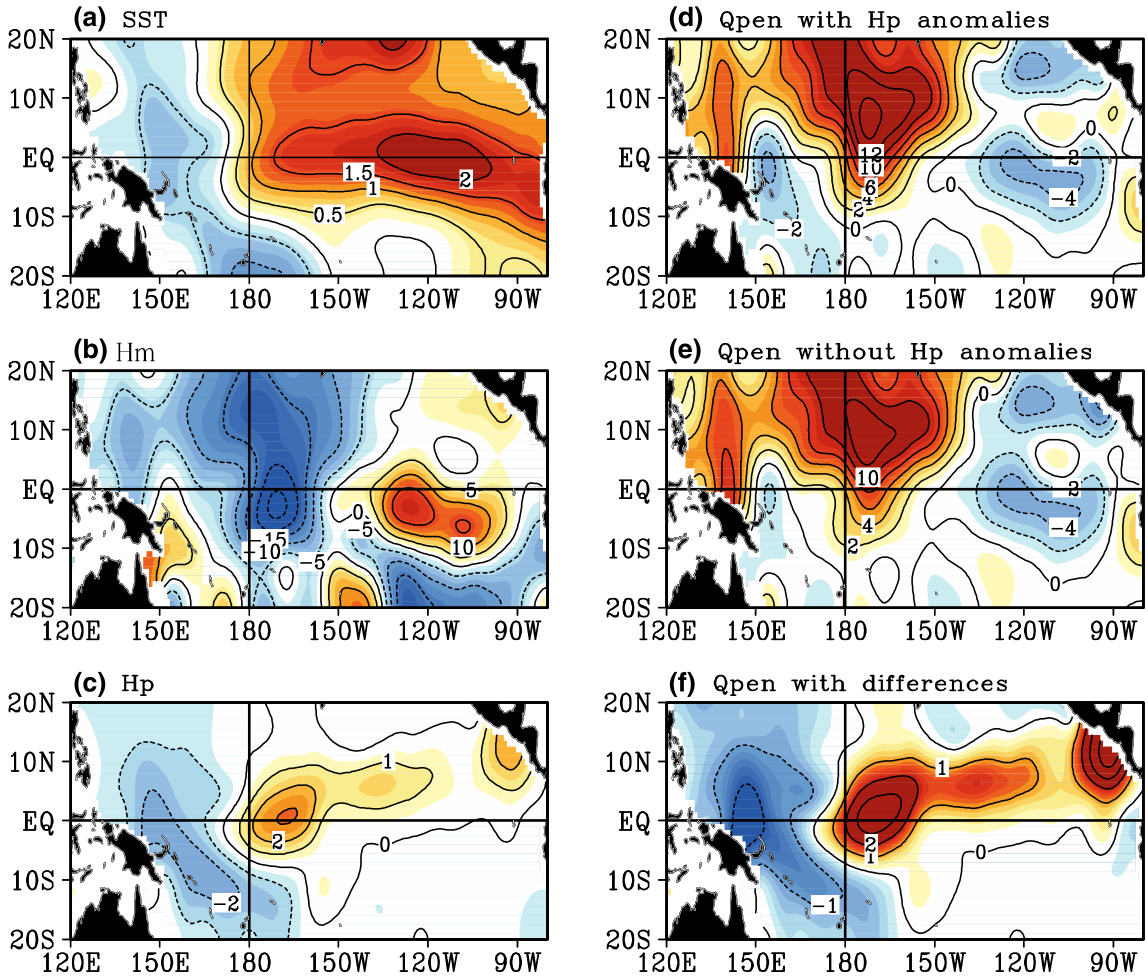

Fig. 9 Same as in Fig. 8 but for El Niño conditions as represented in August 2015

(Fig. 7c), Q_{abs} (Fig. 11a), and R_{sr} (Fig. 12a) indicates that the inter-annual variations in R_{sr} do not follow those in Q_{abs}. In fact, their variations in Q_{abs} and R_{sr} tend to be out of phase in the western-central regions during ENSO cycles. This result indicates that R_{sr} is not determined by Q_{abs} and that the manner in which Q_{abs} is modulated by H_p is not reflected in R_{sr}. This relationship indicates that R_{sr} is not affected by H_p in a coherent fashion.

On the other hand, R_{sr} is closely related to H_m because of their inverse relationship. As such, the manner in which R_{sr} is modulated by H_p can be complicated, which is different from Q_{abs}. Indeed, another factor (the inverse relationship of R_{sr} with H_m) must be considered, which can play an important role in determining the nature of the inter-annual variability of R_{sr}. We provide additional explanations below.

The mathematical expressions in Eq. 3 indicate that R_{sr} is proportional to Q_{abs} (which increases exponentially with H_m but decreases exponentially with H_p); additionally, R_{sr} is inversely proportional to H_m (appearing as a denominator in $R_{sr} = Q_{abs}/(\rho_0 C_p H_m)$). As such, H_m has two effects on R_{sr}: one is exponential through Q_{abs} and the other is an inverse relationship with H_m. Thus, the manner in which R_{sr} is affected by H_p (which is explicitly represented through Q_{abs}) is complicated by the effect of inter-annual H_m variations. During an El Niño event, for example, H_p exhibits a positive anomaly in the western-central regions, which decreases the solar radiation within the ML (a decrease in Q_{abs}); at the same time, the ML tends to be anomalously shallow (a negative H_m anomaly, which decreases Q_{abs}). This decreased Q_{abs} field (which is caused by the effect from the positive H_p anomaly) now acts on this anomalously shallow ML, so the effect on R_{sr} ($= Q_{abs}/(\rho_0 C_p H_m)$) from the reduced Q_{abs} is offset by that from the shoaling ML. The combined net effects of the reduced Q_{abs} component and negative H_m anomaly produce an R_{sr} value that does not change much. Therefore, R_{sr} is not modulated by positive H_p anomalies as significantly as Q_{abs} is during El Niño, and the sign of induced changes in R_{sr} is not consistent with what can be expected from the inter-annual variability of Q_{abs}.

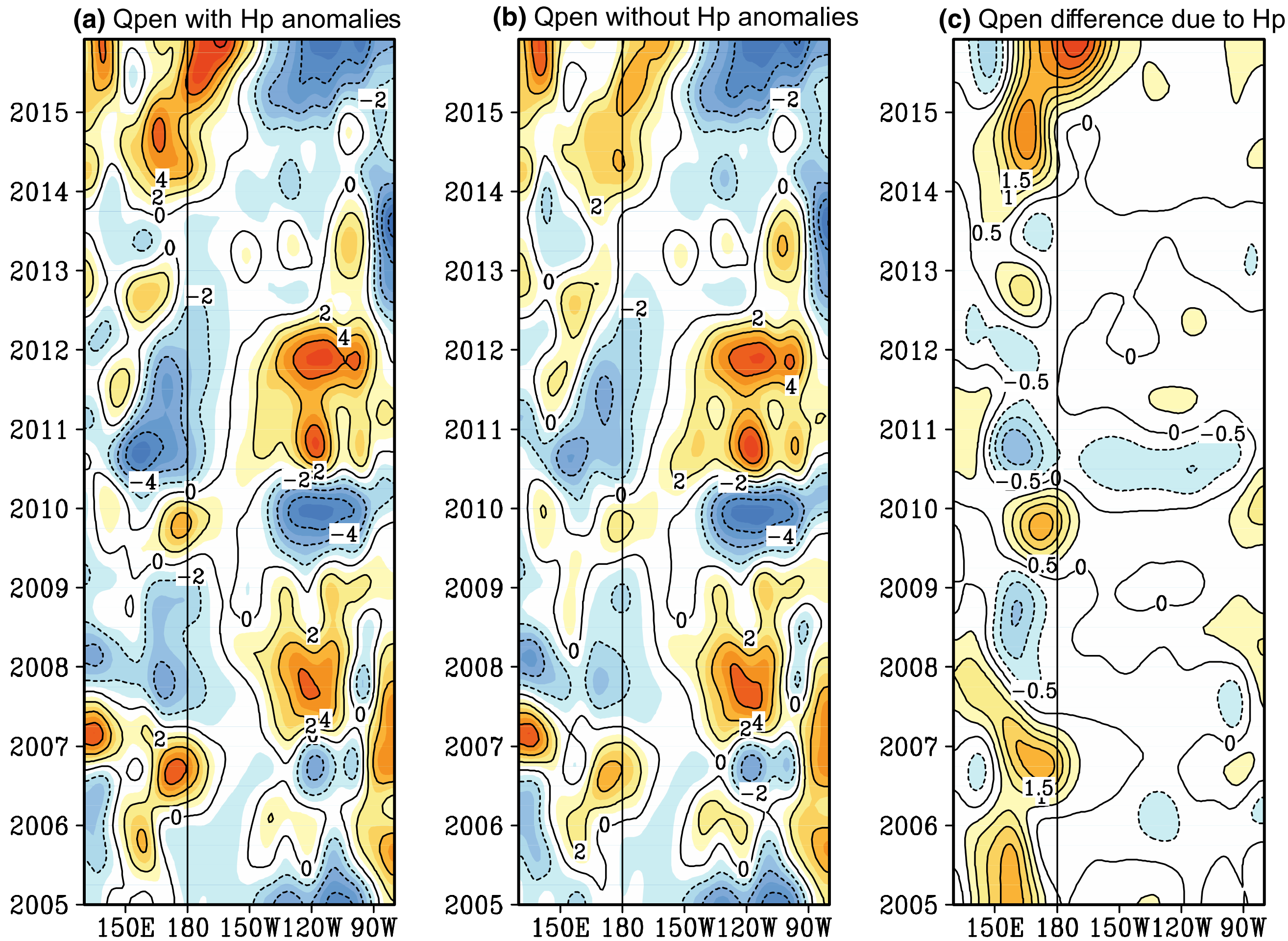

Fig. 10 Time-longitude sections along the Equator during 2005-2015 for inter-annual anomalies: **a** Q_{pen} when estimated with the inter-annual H_p effect considered, **b** Q_{pen} when estimated with the inter-annual H_p effect excluded, and **c** their differences (the Q_{pen} fields estimated with the inter-annual H_p effect included minus those excluded). The contour interval is 2 W m^{-2} in **a** and **b** and 0.5 W m^{-2} in **c**

The relationships among these fields are further quantified in Fig. 13, which presents the anomaly correlations between H_p and Q_{pen} and those between H_p and R_{sr}, respectively. The correlation between H_p and Q_{abs} is exactly the same as that with Q_{pen} but with the opposite sign and is not shown here. Evidently, the extent to which R_{sr} is correlated with H_p is different from what could be inferred from the manner in which Q_{abs} is modulated by H_p, whereas H_p and Q_{pen} (Q_{abs}) indicate a high positive correlation in the western-central equatorial Pacific. One striking feature of H_p and R_{sr} is that these terms are weakly positively correlated in the west, exhibiting the opposite sign to what is expected from the effect of H_p on Q_{abs} (i.e., in terms of the relationship with Q_{abs}, R_{sr} would have a negative correlation with H_p). These results indicate that the extent to which R_{sr} is affected by H_p is different from Q_{abs} and Q_{pen}. The fact that R_{sr} is not significantly modulated by H_p has implications for the manner in which SST is modulated by bio-effects.

3.4 Further attributions to the inter-annual H_p effects

To more clearly understand the bio-effects, further analyses are performed by isolating the contribution from the inter-annual H_p anomalies. The H_p field can be separated into its seasonally varying climatological component ($\overline{H_p}$) and inter-annual component (H_p'); their direct effects on the three heating terms are then explicitly quantified by re-calculating these heating terms (say, Q_{pen}) in two manners, namely, with H_p taken as its seasonally varying climatology (denoted as $Q_{pen}(H_m, \overline{H_p})$) and with H_p considered as varying inter-annually (denoted as $Q_{pen}(H_m, H_p)$). Correspondingly, the effects of the inter-annual H_p anomalies on Q_{pen} can be estimated by calculating the differences between $Q_{pen}(H_m, H_p)$ and $Q_{pen}(H_m, \overline{H_p})$.

Figure 10b, c display the time-longitude sections along the Equator for Q_{pen}; the horizontal patterns for the Q_{pen} difference during El Niño and La Niña are shown in Figs. 8 and

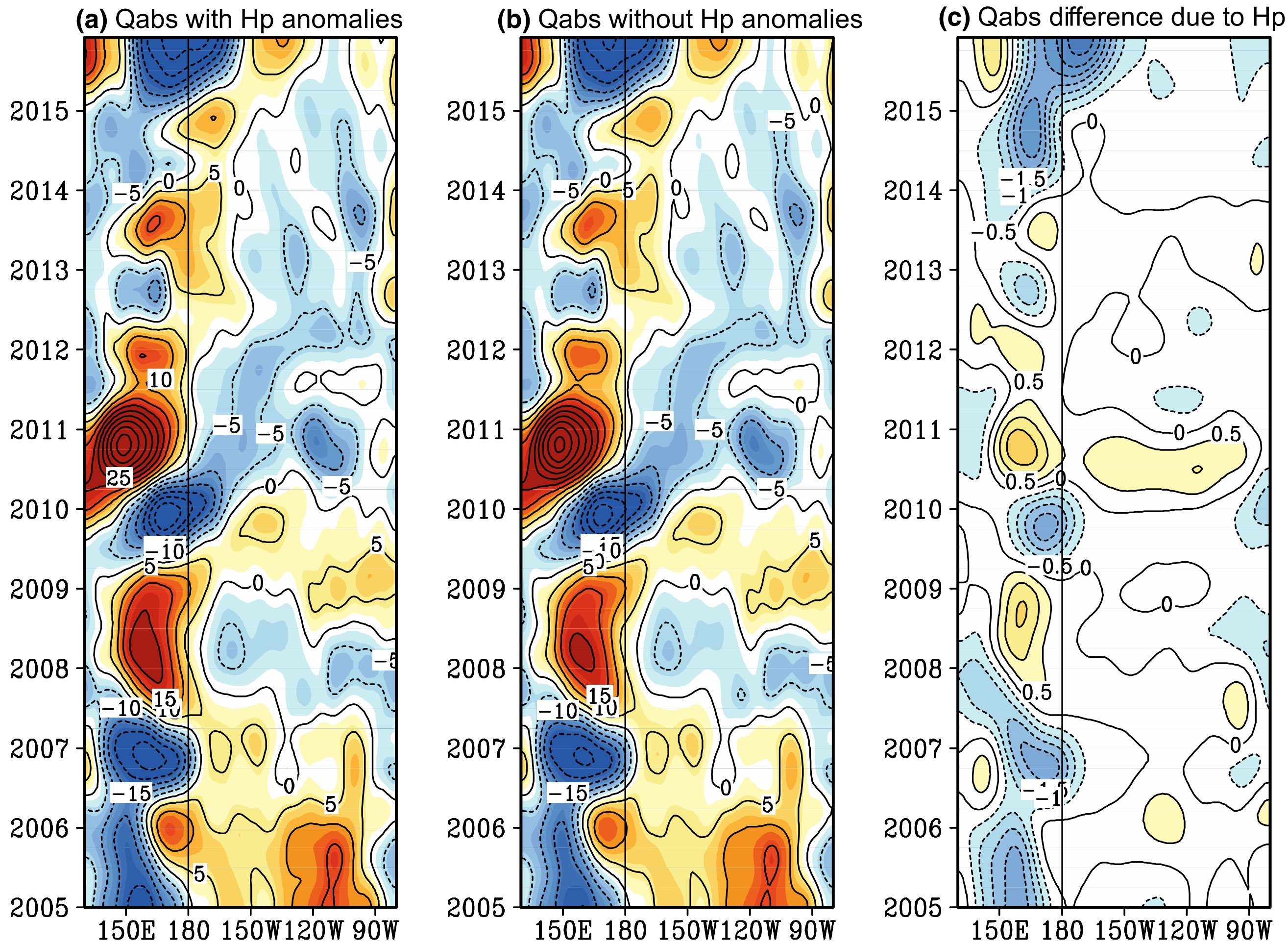

Fig. 11 Time-longitude sections along the Equator during 2005-2015 for inter-annual anomalies: **a** Q_{abs} when estimated with the inter-annual H_p effect considered, **b** Q_{abs} when estimated with the inter-annual H_p effect excluded, and **c** their differences (the Q_{abs} fields estimated with the inter-annual H_p effect included minus those excluded). The contour interval is 5 W m^{-2} in **a** and **b** and 0.5 W m^{-2} in **c**

9. The effects of the inter-annual H_p anomalies on Q_{pen} are mostly pronounced in the western-central equatorial Pacific. High similarities in the spatial patterns and temporal variations are seen between the inter-annual variations in H_p and the Q_{pen} difference. Their relationships indicate that Q_{pen} is significantly modulated by H_p in the western-central regions, where a large variability of H_p exists. The high similarity between H_p and the Q_{pen} difference is consistent with the high positive correlations between the inter-annual variations in H_p and Q_{pen} (Fig. 13).

A similar analysis is performed for Q_{abs}, and the corresponding results are shown in Fig. 11b, c. As defined with Q_{abs} and Q_{pen}, the effects of the inter-annual H_p anomalies on Q_{abs} are the same as for Q_{pen} but with the opposite sign. Good agreement exists between the inter-annual variations in H_p and the Q_{abs} difference, indicating that Q_{abs} is significantly modulated by H_p in the western-central equatorial regions.

Next, we analyze R_{sr}, in which the effects on R_{sr} are estimated by taking H_p as its seasonally varying climatology (denoted as $R_{sr}(H_m, \overline{H_p})$) and varying inter-annually (denoted as $R_{sr}(H_m, H_p)$). Figure 12b, c show the time-longitude sections along the Equator for inter-annual anomalies of $R_{sr}(H_m, \overline{H_p})$ and the differences. The relationships between H_p and the difference field in R_{sr} are different from those in Q_{pen}. A large inter-annual anomaly of H_p does not produce a correspondingly large difference in R_{sr}, indicating that the H_p-induced modulating effect on R_{sr} is weak. The sign of the R_{sr} difference is even opposite to what is expected from the inter-annual H_p effect on Q_{abs}. This result is consistent with the low correlation between H_p and R_{sr}.

Table 1 quantifies the modulating effects of the inter-annual H_p anomalies by calculating the standard deviation of some related variables in the Niño4 region (160°E–150°W, 5°S–5°N). Although the amplitude of the inter-annual variability of H_p is approximately 13% that of H_m in the Niño4

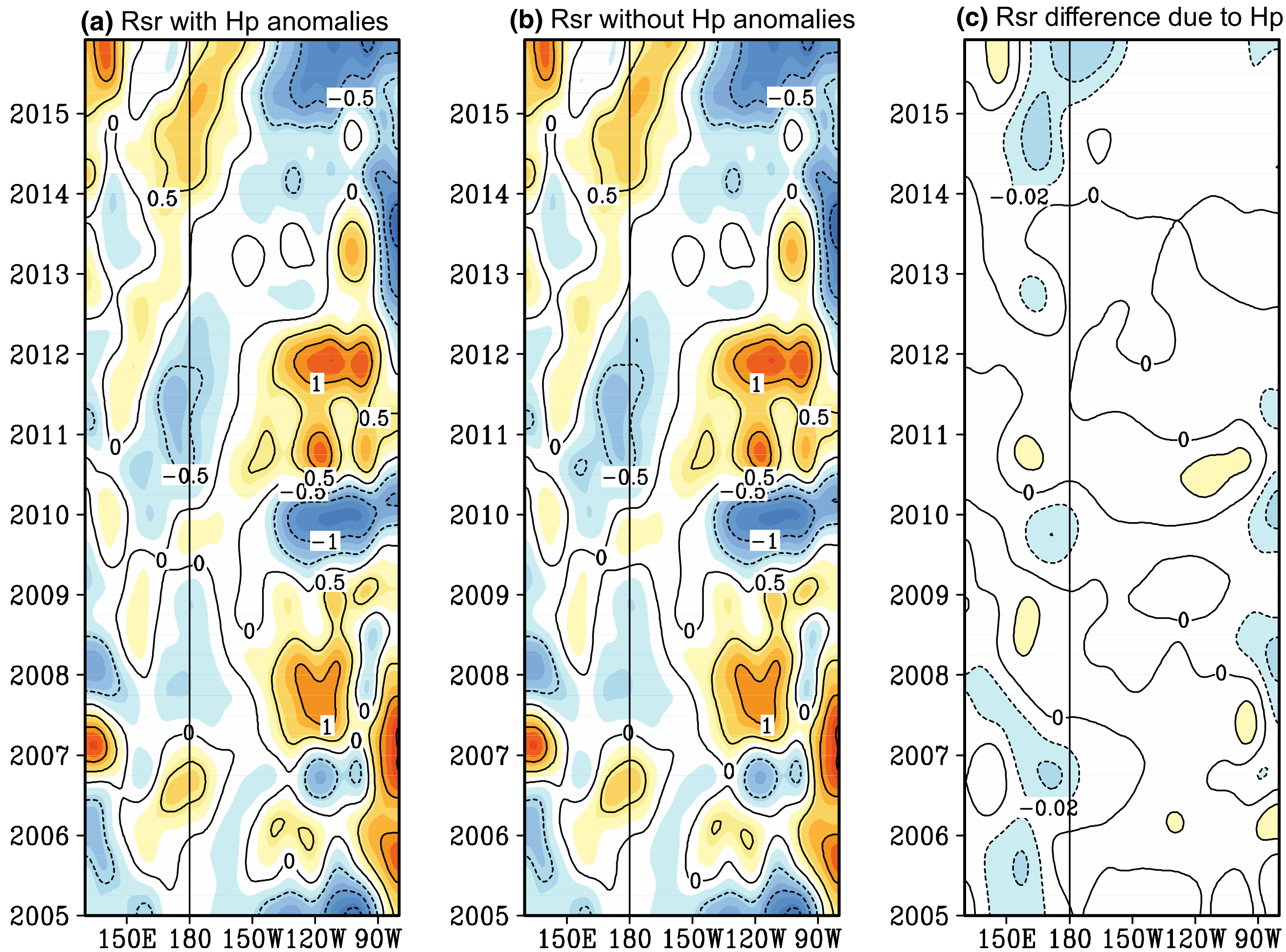

Fig. 12 Time-longitude sections along the Equator for inter-annual anomalies: **a** R_{sr} when estimated with the inter-annual H_p effect considered, **b** R_{sr} when estimated with the inter-annual H_p effect excluded, and **c** their differences (the R_{sr} fields estimated with the inter-annual H_p effect included minus those excluded). The contour interval is 0.5 °C month^{-1} in **a** and **b** and 0.02 °C month^{-1} in **c**

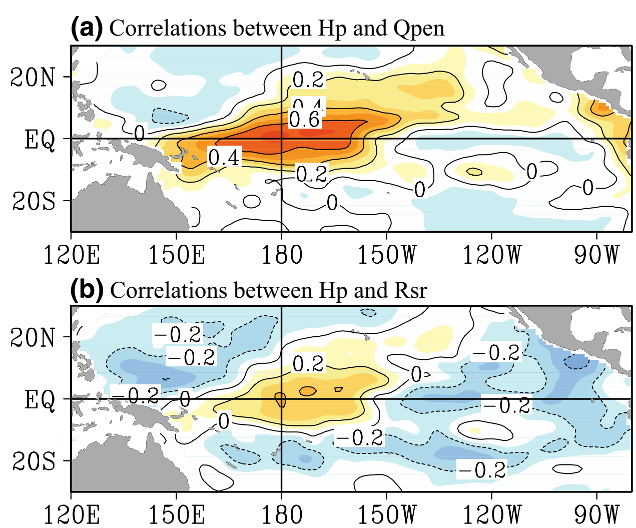

Fig. 13 Correlations during 2005–2015 between inter-annual anomalies of **a** H_p and Q_{pen} and **b** H_p and R_{sr}. The contour interval is 0.2

region, its contribution to the inter-annual variability of Q_{pen} is approximately 28%, whereas that to R_{sr} is only 3%. One interesting feature is that the extent to which R_{sr} is modulated by the inter-annual H_p variability is different from the extent to which Q_{pen} and Q_{abs} are. Quantitatively, the correlation between the inter-annual anomalies of H_p and Q_{pen} is highly positive, and that between H_p and R_{sr} is weakly positive (Fig. 13), indicating that R_{sr} is not modulated as significantly as Q_{abs} and Q_{pen}. The differences in the extent to which these heating terms are modulated by H_p have important implications for the manner in which SST is modulated by bio-effects and the mechanism that is involved.

3.5 Mechanism by which SST is modulated by the OBH feedback

The effects of ocean biology-induced heating on the penetrative solar radiation are realized through the modulations of

Table 1 Standard deviation of variables in the Niño4 region (160°E–150°W, 5°S–5°N)

Variables	H_m (m)	H_p (m)	Q_{pen} with H_p effect ($W\ m^{-2}$)	Q_{pen} without H_p effect ($W\ m^{-2}$)	R_{sr} with H_p effect (°C month^{-1})	R_{sr} without H_p effect (°C month^{-1})
Standard deviation	6.40	0.81	2.55	1.99	0.32	0.33

the three heating terms, which are explicitly related to H_m and H_p. The revealed relationships among these related fields hint at the processes that are involved in the effects of the OBH-related feedback. Two influence pathways are possible by which SST can be modulated by inter-annual variations in H_p in the equatorial Pacific, depending on which heating term is predominantly affected. One is a direct influence pathway by which SST can be modulated through a direct gain or loss in solar radiation within the ML, which is indicated by Q_{abs} and R_{sr}. If a significant change to R_{sr} is induced from Q_{abs} in association with inter-annual H_p anomalies, a direct modulating effect on SST is indicated to be important. In this case, the ML is warmed up or cooled down directly by the H_p-induced Q_{abs} contribution. Then, the bio-feedback is considered to be realized primarily through a direct thermal effect on the SST, which should be reflected in R_{sr}.

Another is an indirect influence pathway, by which Q_{pen} and Q_{abs} are significantly modulated by H_p, but R_{sr} is not. Then, differential heating is produced by H_p vertically between the ML (Q_{abs}) and subsurface layers (Q_{pen}), which modifies the vertical thermal contrast, stratification and vertical mixing in the upper ocean, thus affecting the SST. In this case, Q_{pen} and Q_{abs} are significantly modulated by H_p but R_{sr} does not show a coherent change with Q_{abs}, indicating that the direct thermal effect on the SST is not a predominant mechanism for SST modulation by H_p. As such, an indirect dynamical effect on the SST that is associated with Q_{pen} and Q_{abs} is the dominant process. Therefore, the extent to which these heating terms are modulated by H_p can indicate the importance of a direct thermal effect or indirect dynamical effect on the SST (Fig. 14).

Here, one striking feature revealed from observational data is that inter-annual variations in R_{sr} are not significantly

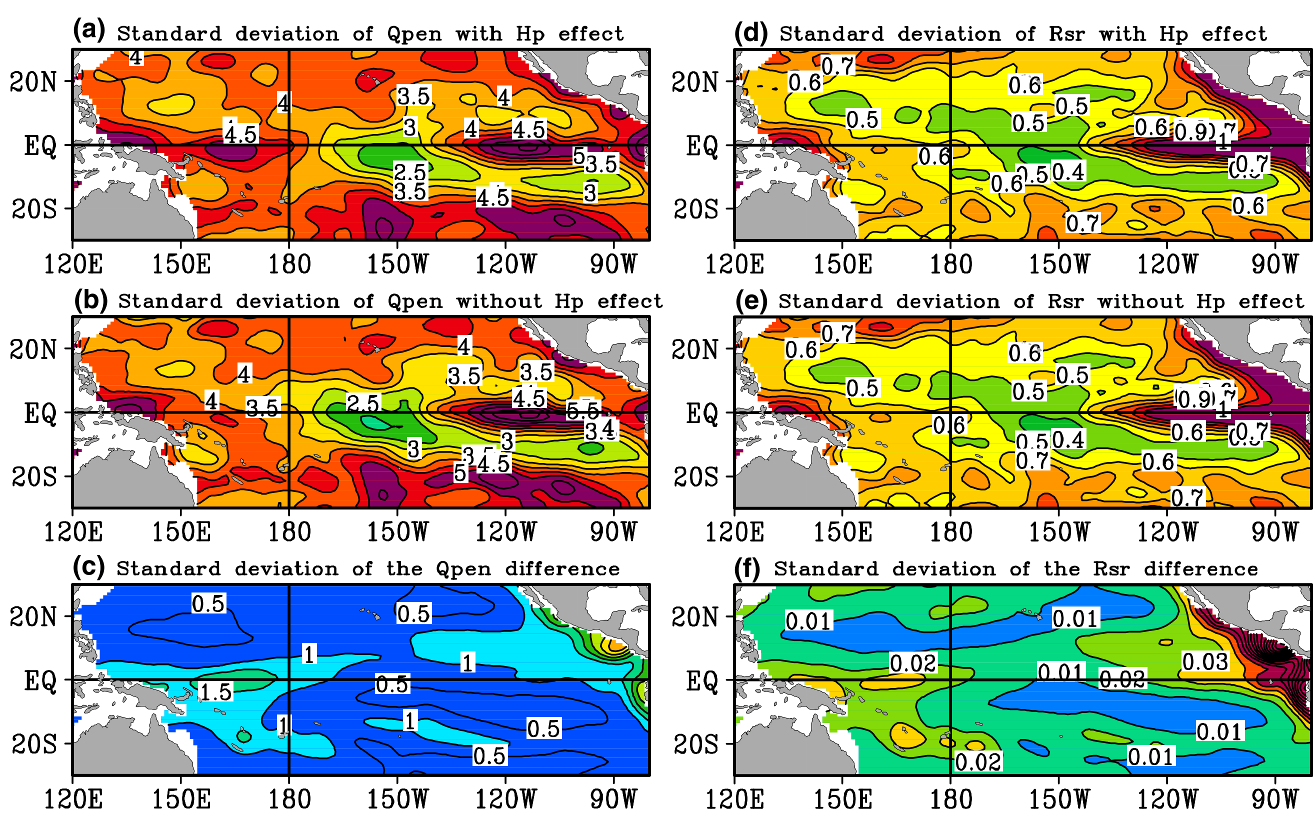

Fig. 14 Standard deviations for inter-annual anomalies of Q_{pen} (left panels) and R_{sr} (right panels), which were estimated with the inter-annual H_p effect (**a**, **d**) considered and (**b**, **e**) excluded, alongside (**e**, **f**) their differences. The contour interval is 0.5 $W\ m^{-2}$ in **a–c**, 0.1 °C month^{-1} in **d** and **e**, and 0.01 °C month^{-1} in **f**

modulated by H_p. That is, R_{sr} does not exhibit a corresponding positive anomaly, as would be expected from the effect of inter-annual H_p anomalies on Q_{abs} in the western-central regions. The effects of H_p on R_{sr} cannot explain the modulating effect on the SST because the sign of the modulating effect on R_{sr} is opposite to what is expected from the inter-annual H_p effect on Q_{abs}. Thus, bio-effects on the SST are not realized through the R_{sr} term. Other processes that are involved in the effects on Q_{pen} and Q_{abs} must play a dominantly important role in modulating the SST. Indeed, the inter-annual variability of H_p acts to enhance that of Q_{abs} and Q_{pen} during ENSO cycles. The H_p-enhanced anomalies of Q_{abs} and Q_{pen} produce large differential heating between the ML and subsurface layers, which modulates the vertical thermal contrast, stratification and vertical mixing, which represent a dominant indirect ocean dynamical effect on the SST.

4 Summary and discussion

In this paper, observed data were used to characterize the inter-annual variabilities of related physical and biological oceanic fields in the tropical Pacific. In terms of ocean biology, Chl anomalies appeared very quickly and almost simultaneously as a response to ENSO cycles. For example, large inter-annual variations in Chl were concentrated in the western-central equatorial Pacific near the date line: low-Chl-concentration regions extended eastward across the date line during El Niño but retreated westward during La Niña. These inter-annual variations in Chl both represented a response to the ENSO and exhibited feedback onto the ENSO. Here, Chl was considered a major component that affected the vertical penetration of solar radiation in the upper ocean and represented the bio-heating feedback; then, Chl was used to derive the penetration depth (H_p) and quantify the effect on the penetrative solar radiation. In terms of physical factors, H_m was estimated from Argo products. As with H_p, H_m exhibited large inter-annual anomalies in response to ENSO cycles. The incoming shortwave radiation decayed exponentially with depth in the upper ocean, so H_m was a major factor that controlled the penetration of solar radiation in the upper ocean. Thus, H_m and H_p are two factors that affect the distribution of solar radiation between the ML and the underlying subsurface layers.

To quantify the effects from inter-annual H_p anomalies, three heating terms were explicitly expressed as a function of H_p and H_m (Zhang 2015). As previously demonstrated by modeling studies, the biological conditions can affect the mean climate and inter-annual variability over the tropical Pacific through modulating effects on these heating terms. The structural relationships of H_m and H_p with the related heating terms were analyzed to gain insight into Chl-induced heating effects on the ENSO in nature. Furthermore, the revealed relationships from observations could be inferred to determine the processes and mechanisms for ENSO modulations.

The ENSO can induce large perturbations to H_p and H_m, whose inter-annual variations exhibited a well-defined structure across the tropical Pacific. H_p and H_m directly affected the three heating terms (Q_{pen}, Q_{abs} and R_{sr}), which underwent inter-annual variations that were dominated by ENSO signals. A combined modulating effect from H_m and H_p was seen on Q_{pen}. In the western-central equatorial region, the inter-annual variations in H_p were large and have an out-of-phase relationship with those in H_m during ENSO cycles. The effects on Q_{pen} induced by inter-annual anomalies of H_p tended to be of the same sign as those of H_m, with a high positive correlation between H_p and Q_{pen}. During El Niño, for example, Q_{pen} exhibited a positive anomaly, which can be attributed to the negative H_m anomaly. At this time, H_p was positive. The effect of this positive H_p anomaly caused the positive Q_{pen} anomaly during El Niño to become more positive. During La Niña, Q_{pen} became a negative anomaly in association with a positive H_m anomaly. At the same time, H_p became a negative anomaly, which caused the negative Q_{pen} anomaly to become more negative. So, the inter-annual anomalies of H_p enhanced those of Q_{pen}. In terms of Q_{abs}, the H_p effect was the same as with Q_{pen} but with the opposite sign. That is, in the western-central equatorial Pacific, the effects of the positive H_p anomaly during El Niño made the negative Q_{abs} more negative, whereas those of the negative H_p anomaly made the positive Q_{abs} more positive during La Niña. Thus, the inter-annual H_p anomalies enhanced the differential heating between the ML (Q_{abs}) and subsurface layers (Q_{pen}). In terms of the effect on R_{sr}, the extent to which R_{sr} was modulated by H_p was strikingly different from Q_{pen} and Q_{abs}. Although Q_{abs} and Q_{pen} were significantly modulated by H_p, R_{sr} was not. So, the modulating effects of H_p on the SST were not realized through the R_{sr} term and a direct thermal effect from H_p through Q_{abs} was not a major process that modulated the SSTs. In contrast, Q_{pen} and Q_{abs} were significantly modulated by H_p in the western-central equatorial Pacific. As such, the H_p-enhanced anomalies of Q_{pen} and Q_{abs} produced large differential heating between the ML and subsurface layers, which modified the vertical thermal contrast, stratification and vertical mixing, thus affecting the SST. Thus, the modulating effects of H_p on the SST can be traced to the Q_{pen} and Q_{abs} terms, and bio-modulations of the ENSO were realized through an indirect dynamical effect on the SST in association with inter-annual H_p anomalies. Furthermore, the structural relationships indicated a negative feedback on the ENSO.

In this study, satellite-based Chl data were combined with Argo data to estimate inter-annual variations in H_p and H_m. Furthermore, the derived H_p and H_m fields were used to

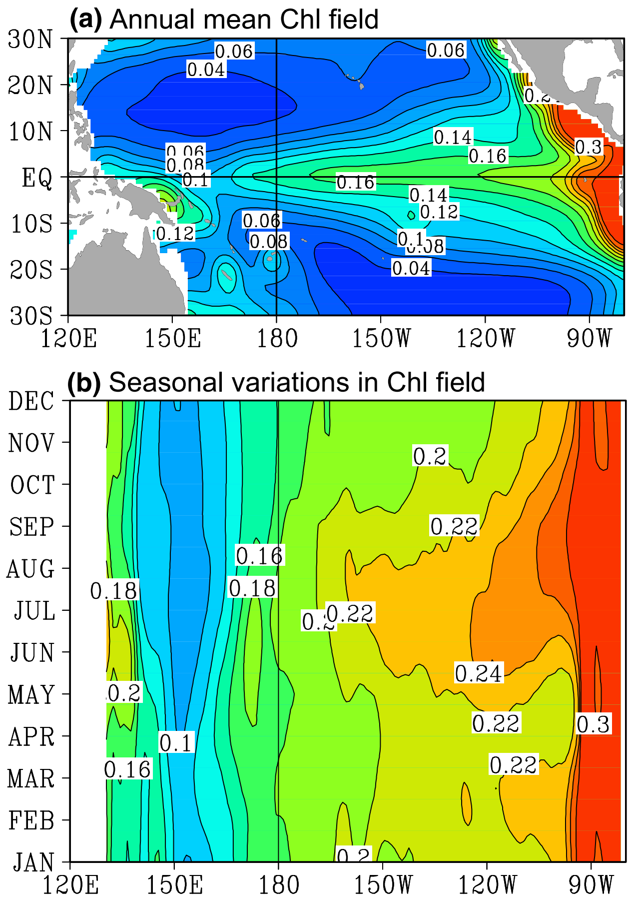

Fig. 15 Estimated Chl fields during 2005–2015 from satellite observations: **a** horizontal distribution for the annual mean climatology and **b** seasonal variations along the Equator. The contour interval is 0.02 mg m^{-3} in **a** and **b**

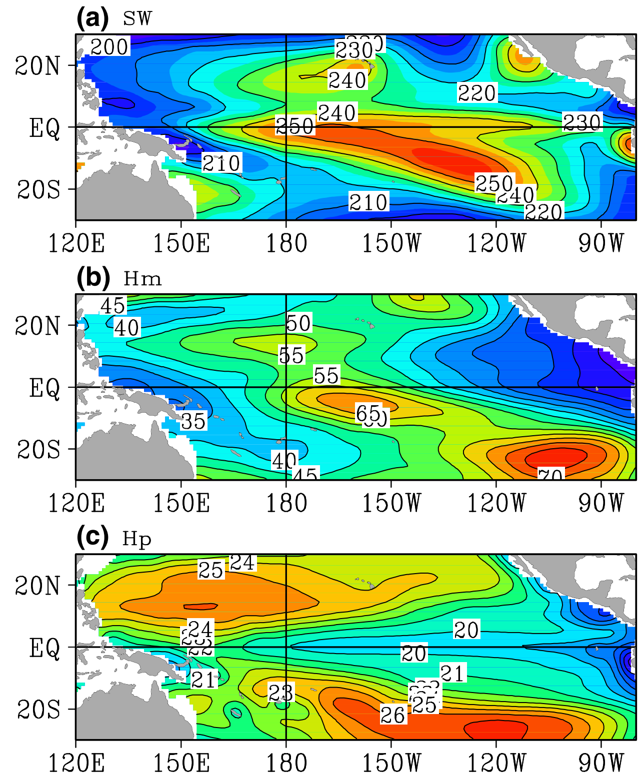

Fig. 16 Horizontal distributions of the annual-mean fields during 2005–2015: **a** shortwave radiation from MERRA, **b** H_m from the Argo product, and **c** H_p from the GlobColour Project. The contour interval is 10 W m^2 in **a**, 5 m in **b**, and 1 m in **c**

reveal their effects on ocean biology-induced heating terms and the modulating effects on the SST. The added values of satellite-Chl observations were clearly demonstrated in association with the use of in situ data. This use of satellite and in situ data elucidated the observed structural relationships among the related fields and processes that were involved in the bio-effects. In particular, an indirect dynamical effect on the SST from the inter-annual Chl variability could explain a negative feedback on the ENSO in the tropical Pacific.

These structural relationships in nature provide an observational basis for validating model simulations (Gnanadesikan and Anderson 2009; Jochum et al. 2010; Kang et al. 2017a; Zhi et al. 2019). For example, in our previous modeling studies, a statistical approach was utilized to derive a model for the inter-annual variations in H_p from satellite observations of Chl and H_p. The observational analyses from this study indicated a good relationship between the inter-annual variations in Chl (H_p) and the SST, so adopting a statistical approach was justified here. Furthermore, the derived H_p statistical model was used for coupled ocean–atmosphere simulations, and the relationships among these fields and modulating effects on the ENSO in modeling studies were consistent with this observation-based analysis. The results from these observation-based analyses support our previous modeling studies using the statistical H_p approach. By combining these observations and previous modeling, the modulating effects of ocean biology-induced heating were clearly demonstrated with a negative feedback on the ENSO. Furthermore, an indirect dynamical effect from inter-annual anomalies of H_p was identified as the predominant mechanism for ENSO modulations. These analyses offer a clear method to trace the influence pathways through which the ENSO is modulated by Chl anomalies, and the methodology that was developed in this study can be used in other models to reveal bio-effects.

In this study, we demonstrated the relationships between inter-annual variability of Chl and ENSO modulations using observational data. A diagnostic analysis is performed to quantify the contribution of interannual H_p anomalies to the three heating terms in association with that of H_m. Note that large inter-annual variability of Chl is located in the western-central equatorial Pacific. As seen in this analysis, the ENSO is a clear source for the Chl variability that is strongly affected by the upwelling and mixing processes

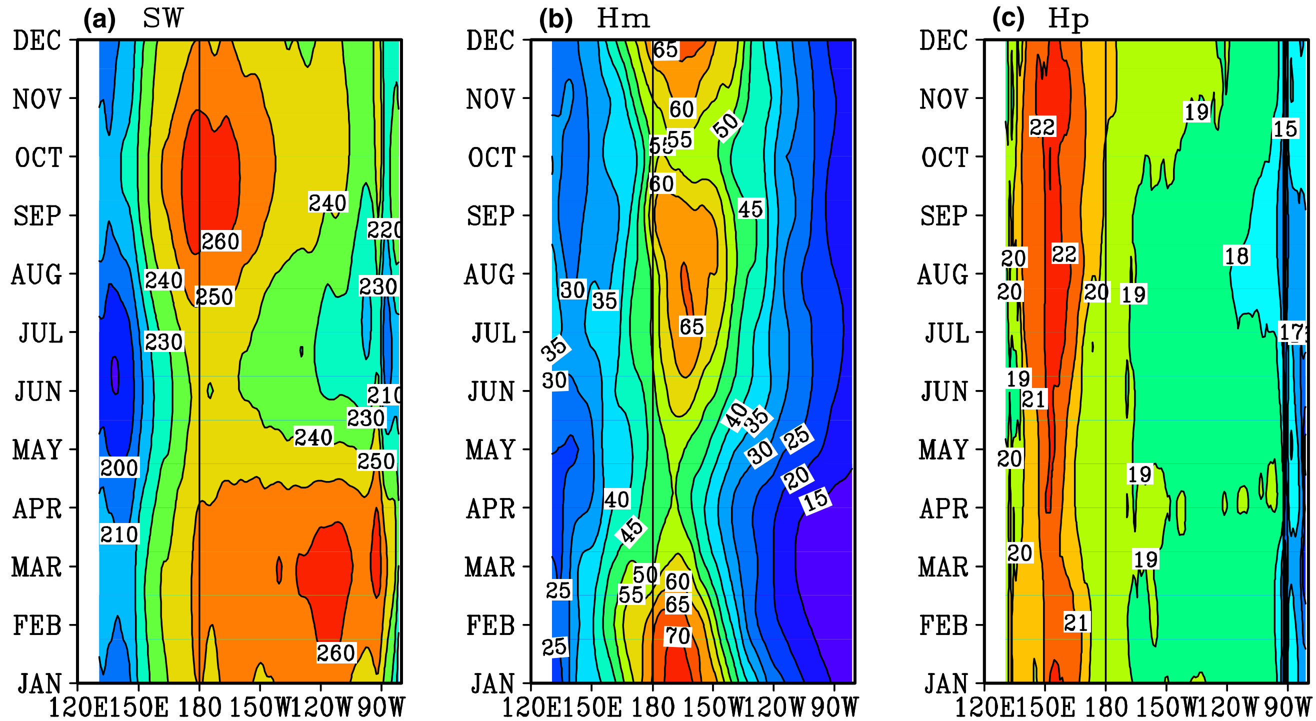

Fig. 17 Seasonal variations along the Equator for climatological fields during 2005–2015: **a** shortwave radiation, **b** H_m, and **c** H_p. The contour interval is 10 W m^{-2} in **a**, 5 m in **b**, and 1 m in **c**

in the region. However, the detailed processes that can be responsible for inter-annual variability of Chl have not been analyzed from this observations-based analysis. Also, we present a clear explanation for understanding the feedback onto ENSO induced by inter-annual Chl variability. But, here we only considered the direct impact of H_p on interannual variations of these related heat items using a diagnostic method. In fact, through the modulating effects on stratification and mixing, H_p is expected to have an impact on H_m, and thus there exist interactions between interannual variations in H_p and H_m. These issues cannot be evaluated from this observational analysis, and thus need to be addressed further by modeling studies as shown in (Zhang et al. 2018a, b, 2019).

Acknowledgements The author would like to thank Drs. Mu Mu, Dunxin Hu, Fan Wang, Dake Chen, Anand Gnanadesikan, Tony Busalacchi, Youmin Tang, and Zhaohua Wu for their comments. The authors wish to thank the anonymous reviewers for their numerous comments that helped to improve the original manuscript. This research was supported by the National Programme on Global Change and Air–Sea Interaction (Grant No. GASI-IPOVAI-06), the Strategic Priority Research Program of the Chinese Academy of Sciences (Grant No. XDA19060102), National Natural Science Foundation of China (Grant Nos. 41690122(41690120), 41490644(41490640), 41421005), the NSFC-Shandong Joint Fund for Marine Science Research Centers (U1406402) and the Taishan Scholarship. Zhi is additionally supported by the Foundation of Key Laboratory of Ocean Circulation and Waves (KLOCW), IOCAS (KLOCW1601), and Kang is additionally supported by the Foundation of KLOCW, IOCAS (KLOCW1809).

Appendix: Mean state and seasonal variations

Observations are used to analyze the structure and variability of ocean biology-related heating effects in the tropical Pacific, including Chl, H_p, H_m, short wave (SW) solar radiation, and the three heating terms. The three heating terms, which were derived from combined satellite and in situ data, are new fields that have not been shown before. In this Appendix, we present the mean state and seasonal variabilities of these related fields to support the inter-annual variability analyses in the main text.

A1. Chl field

Figure 15 displays the annual-mean field of Chl and its variations in the equatorial Pacific according to satellite measurements. The magnitude of the seasonal and inter-annual Chl variabilities is comparable to that of its total value. The main characteristics of Chl are clearly evident in Fig. 1b and Fig. 15a, as previously described (e.g., Ballabrera-Poy et al. 2007). For example, a pronounced ridge is seen in the equatorial regions, with high Chl values extending from the east to the west along the Equator. The Chl concentration is low (< 0.1 mg m^{-3}) in the western equatorial Pacific in association with warm waters and high in the central and eastern equatorial regions, where a cold tongue develops.

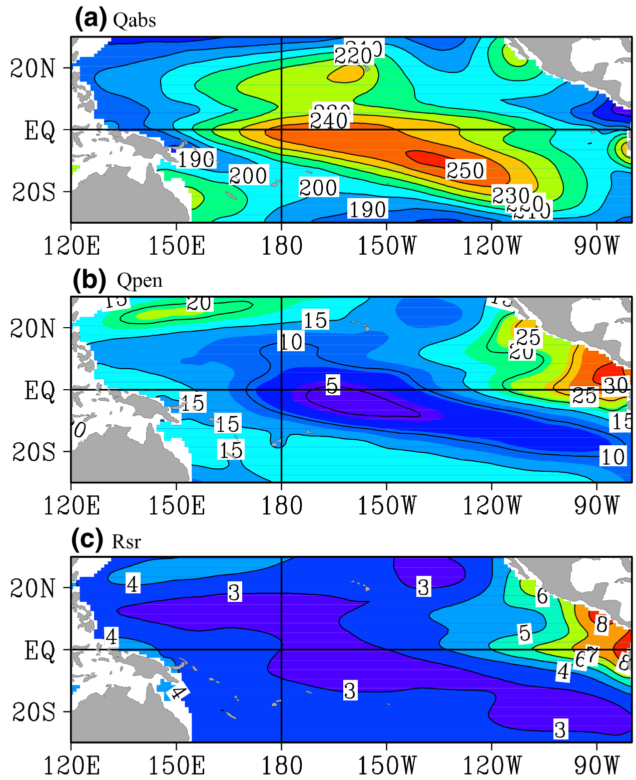

Fig. 18 Horizontal distributions of the annual-mean fields during 2005-2015 for ocean Chl-related heating terms: **a** Q_{abs}, **b** Q_{pen}, and **c** R_{sr}. The contour interval is 10 W m^{-2} in **a**, 5 W m^{-2} in **b** and 1 °C month^{-1} in **c**

In the far-eastern coastal regions, the Chl concentration is especially high. Correspondingly, large gradients exist in the western equatorial region and far-eastern region.

The annual-mean Chl field and corresponding seasonal variability of Chl along the Equator are shown in Fig. 15. Longitudinally, Chl exhibits elevated values from west to east across the equatorial Pacific. Large seasonal variations in Chl are seen in the western-central equatorial Pacific, with a pronounced peak in summer. In the eastern equatorial region, low values are observed in spring and high values in summer. These seasonal variations in Chl are associated with those in physical conditions in the equatorial Pacific (e.g., upwelling and vertical mixing).

A2. Short wave (SW) solar radiation, H_p and H_m

Figure 16a exhibits the horizontal distributions of the average annual-mean shortwave (SW) solar radiation during 2005–2015; its corresponding seasonal variation is shown in Fig. 17a. Regions with large values are seen in the western-central equatorial Pacific and those with low values are seen in the eastern region. Seasonally, solar radiation that reaches the sea surface has a pronounced semiannual cycle along the Equator (Fig. 17a). The SW radiation penetrates the upper ocean.

The corresponding results for the depth of the ML (H_m) are displayed in Figs. 16b and 17b. Regions with a deep ML are located in the western-central equatorial Pacific and

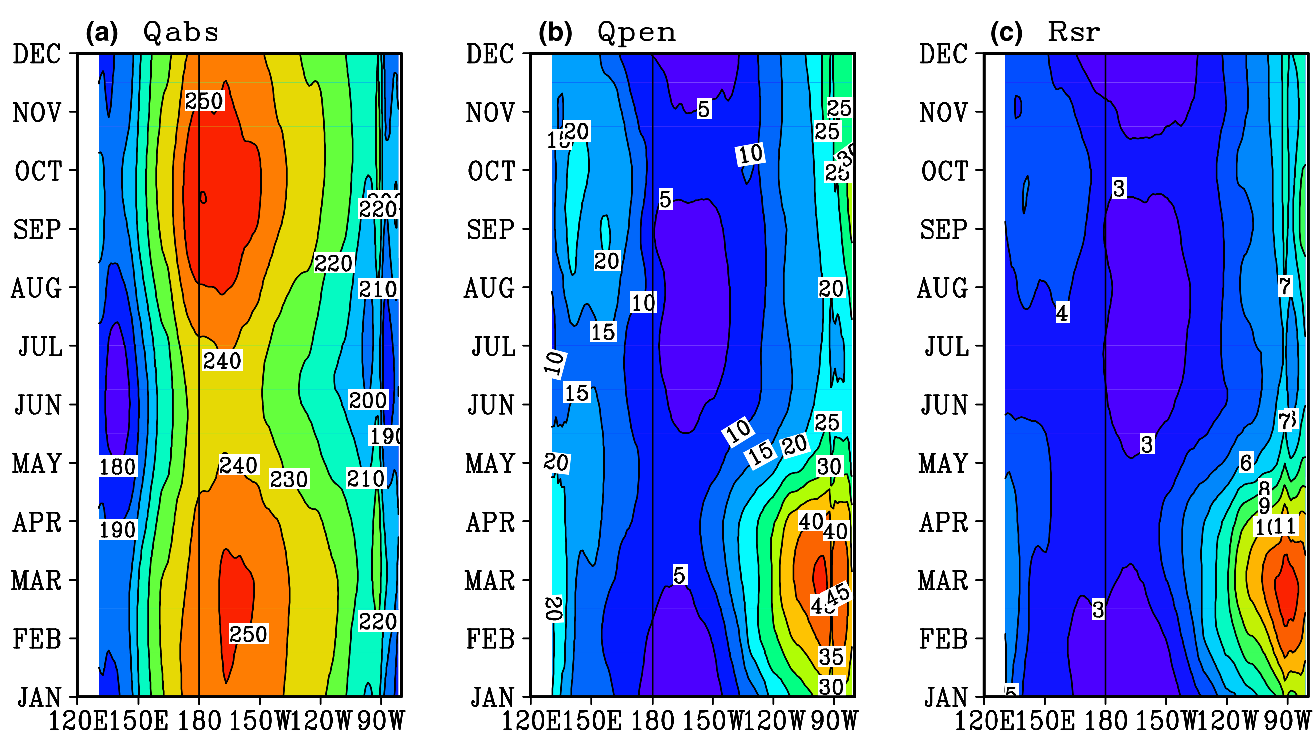

Fig. 19 Seasonal variations along the Equator for the climatological heating terms during 2005–2015: **a** Q_{abs}, **b** Q_{pen}, and **c** R_{sr}. The contour interval is 10 W m^{-2} in **a**, 5 W m^{-2} in **b** and 1 °C month^{-1} in **c**

those with a shallow ML are seen in the western and eastern regions. In both the western and eastern sides of the tropical Pacific and the Intertropical Convergence Zone (ITCZ), the ML is relatively shallow because of the weak surface friction velocity and the stabilizing surface buoyancy flux. Values larger than 50 m are found in the central tropical regions, where surface winds are energetic with strong surface buoyancy losses. Seasonal variations are clearly evident. In the eastern equatorial region, the ML is shallow in spring and deep in fall. In the western equatorial basin, the ML is deep in winter but shallow in the late spring.

Chl is used to derive the penetration depth (H_p), and its annual-mean structure is shown in Fig. 15a. A pronounced trough is seen in the equatorial regions, with low H_p values extending from east to west along the Equator. Deep penetration depths with values larger than 20 m are observed in the western equatorial Pacific, while shallow penetration depths are found in the east. Large gradients are located in the western equatorial Pacific and far-eastern regions. Seasonally, the solar radiation exhibits deep penetration in spring and shallow penetration in fall.

A3. Three heating terms (Q_{abs}, Q_{pen} and R_{sr})

As mathematically expressed above, SW, H_p and H_m all determine the distributions of penetrative solar radiation between the mixed layer and the underlying subsurface layers. The annual-mean structures of these three heating terms are shown in Fig. 18, and the corresponding seasonal variations are displayed in Fig. 19. The magnitude of the total Q_{abs} and Q_{pen} fields is one order larger than that of their interannual variabilities. Most of the solar radiation is absorbed within the ML (Fig. 18a), with some penetrating through the bottom of the ML (Fig. 18b). These terms exhibit coherent relationships with SW, H_m and H_p. For example, the structure and magnitude of Q_{abs} is similar to those of SW; Q_{pen} has low values in the western-central equatorial Pacific and high values in the western and eastern equatorial Pacific. Q_{abs}, Q_{pen} and R_{sr} all have a clear signature for H_m, so H_m is major factor that affects the penetration of solar radiation. Seasonally, Q_{abs} has a pronounced semiannual cycle along the equator (Fig. 19a), similar to the SW solar radiation reaching the sea surface. Interestingly, seasonal variations in Q_{pen} and R_{sr} (Fig. 19b, c) exhibit a slight shift in time compared to Q_{abs} (Fig. 19c). The seasonal variations in these heating terms indicate that these terms are predominantly determined by H_m. No clear signature is seen for the effect of H_p on these heating terms in terms of the mean field and seasonal variations.

Thus, H_m is a major factor that controls the distribution of solar radiation within the ML and subsurface layers. As such, if the ML is deeper, SW solar radiation is absorbed more within the ML and penetrates less into the subsurface layers. If the ML is deep enough, all the radiation would be absorbed within the ML, with little penetration through the bottom of the ML. In such a situation, H_p would barely influence the penetrative solar radiation in the upper ocean.

References

Anderson W, Gnanadesikan A, Wittenberg A (2009) Regional impacts of ocean color on tropical Pacific variability. Ocean Sci 5:313–327. https://doi.org/10.5194/os-5-313-2009

Ballabrera-Poy J, Murtugudde R, Zhang R-H, Busalacchi AJ (2007) Coupled Ocean-Atmosphere response to seasonal modulation of ocean color: impact on interannual climate simulations in the Tropical Pacific. J Clim 20:353–374. https://doi.org/10.1175/JCLI3958.1

Gnanadesikan A, Anderson WG (2009) Ocean water clarity and the ocean general circulation in a coupled climate model. J Phys Oceanogr 39:314–332. https://doi.org/10.1175/2008JPO3935.1

Jochum M, Yeager S, Lindsay K et al (2010) Quantification of the feedback between phytoplankton and ENSO in the community climate system model. J Clim 23:2916–2925. https://doi.org/10.1175/2010JCLI3254.1

Kang X, Zhang R-H, Gao C, Zhu J (2017a) An improved ENSO simulation by representing chlorophyll-induced climate feedback in the NCAR Community Earth System Model. Sci Rep 7:17123. https://doi.org/10.1038/s41598-017-17390-2

Kang X, Zhang R-H, Wang G (2017b) Effects of different freshwater flux representations in an ocean general circulation model of the tropical Pacific. Sci Bull 62:345–351. https://doi.org/10.1016/j.scib.2017.02.002

Lee T, McPhaden MJ (2010) Increasing intensity of El Niño in the central-equatorial Pacific. Geophys Res Lett. https://doi.org/10.1029/2010gl044007

Lengaigne M, Menkes C, Aumont O et al (2007) Influence of the oceanic biology on the tropical Pacific climate in a coupled general circulation model. Clim Dyn 28:503–516. https://doi.org/10.1007/s00382-006-0200-2

Lewis MR, Carr M-E, Feldman GC et al (1990) Influence of penetrating solar radiation on the heat budget of the equatorial Pacific Ocean. Nature 347:543–545. https://doi.org/10.1038/347543a0

Maritorena S, D'Andon OHF, Mangin A, Siegel DA (2010) Merged satellite ocean color data products using a bio-optical model: characteristics, benefits and issues. Remote Sens Environ 114:1791–1804. https://doi.org/10.1016/j.rse.2010.04.002

Marzeion B, Timmermann A, Murtugudde R, Jin F-F (2005) Biophysical feedbacks in the tropical pacific. J Clim 18:58–70. https://doi.org/10.1175/JCLI3261.1

McClain CR, Cleave ML, Feldman GC, Gregg WW, Hooker SB, Kuring N (1998) Science quality SeaWiFS data for global biosphere research. Sea Technol 39:10–16

Morel A, Antoine D (1994) Heating rate within the upper ocean in relation to its bio–optical state. J Phys Oceanogr 24:1652–1665

Murtugudde R, Beauchamp J, McClain CR et al (2002) Effects of penetrative radiation on the upper tropical ocean circulation. J Clim 15:470–486. https://doi.org/10.1175/1520-0442(2002)015%3c0470:EOPROT%3e2.0.CO;2

Park J-Y, Kug J-S, Seo H, Bader J (2014) Impact of bio-physical feedbacks on the tropical climate in coupled and uncoupled GCMs. Clim Dyn 43:1811–1827. https://doi.org/10.1007/s00382-013-2009-0

Philander S (1983) El Niño southern oscillation phenomena. Nature 302:295–301. https://doi.org/10.1038/302295a0

Reynolds RW, Rayner NA, Smith TM et al (2002) An improved in situ and satellite SST analysis for climate. J Clim 15:1609–1625. https://doi.org/10.1175/1520-0442(2002)015%3c1609:AIISAS%3e2.0.CO;2

Rienecker MM, Suarez MJ, Gelaro R et al (2011) MERRA: NASA's modern-era retrospective analysis for research and applications. J Clim 24:3624–3648. https://doi.org/10.1175/JCLI-D-11-00015.1

Siegel DA, Maritorena S, Nelson NB et al (2002) Global distribution and dynamics of colored dissolved and detrital organic materials. J Geophys Res 107:1–14. https://doi.org/10.1029/2001jc000965

Strutton PG, Chavez FP (2004) Biological heating in the equatorial pacific: observed variability and potential for real-time calculation. J Clim 17:1097–1109. https://doi.org/10.1175/1520-0442(2004)017%3c1097:BHITEP%3e2.0.CO;2

Tang Y, Zhang R-H, Liu T et al (2018) Progress in ENSO prediction and predictability study. Natl Sci Rev 5:826–839. https://doi.org/10.1093/nsr/nwy105

Timmermann A, Jin F-F (2002) Phytoplankton influences on tropical climate. Geophys Res Lett 29:19-1–19-4. https://doi.org/10.1029/2002gl015434

Wang XJ, Le Borgne R, Murtugudde R et al (2008) Spatial and temporal variations in dissolved and particulate organic nitrogen in the equatorial Pacific: biological and physical influences. Biogeosciences 5:1705–1721. https://doi.org/10.5194/bg-5-1705-2008

Wetzel P, Maier-Reimer E, Botzet M et al (2006) Effects of ocean biology on the penetrative radiation in a coupled climate model. J Clim 19:3973–3987. https://doi.org/10.1175/JCLI3828.1

Zebiak SE, Cane MA (1987) A model El Niño–southern oscillation. Mon Weather Rev 115:2262–2278. https://doi.org/10.1175/1520-0493(1987)115%3c2262:AMENO%3e2.0.CO;2

Zhang R-H (2015) Structure and effect of ocean biology-induced heating (OBH) in the tropical Pacific, diagnosed from a hybrid coupled model simulation. Clim Dyn 44:695–715. https://doi.org/10.1007/s00382-014-2231-4

Zhang R-H, Busalacchi AJ (2008) Rectified effects of tropical instability wave (TIW)-induced atmospheric wind feedback in the tropical Pacific. Geophys Res Lett 35:1–6. https://doi.org/10.1029/2007GL033028

Zhang R-H, Busalacchi AJ (2009) Freshwater flux (FWF)-induced oceanic feedback in a hybrid coupled model of the tropical Pacific. J Clim 22:853–879. https://doi.org/10.1175/2008JCLI2543.1

Zhang R-H, Gao C (2016) The IOCAS intermediate coupled model (IOCAS ICM) and its real-time predictions of the 2015–2016 El Niño event. Sci Bull 61:1–10. https://doi.org/10.1007/s11434-016-1064-4

Zhang R-H, Levitus S (1997) Structure and cycle of decadal variability of upper-ocean temperature in the North Pacific. J Clim 10:710–727. https://doi.org/10.1175/1520-0442(1997)010%3c0710:SACODV%3e2.0.CO;2

Zhang R-H, Busalacchi AJ, Wang X et al (2009) Role of ocean biology-induced climate feedback in the modulation of El Niño-Southern Oscillation. Geophys Res Lett. https://doi.org/10.1029/2008gl036568

Zhang R-H, Chen D, Wang G (2011) Using satellite ocean color data to derive an empirical model for the penetration depth of solar radiation (Hp) in the tropical Pacific ocean. J Atmos Ocean Technol 28:944–965. https://doi.org/10.1175/2011JTECHO797.1

Zhang R-H, Zheng F, Zhu J et al (2012) Modulation of El Niño-Southern Oscillation by freshwater flux and salinity variability in the tropical Pacific. Adv Atmos Sci 29:647–660. https://doi.org/10.1007/s00376-012-1235-4

Zhang R-H, Tian F, Wang X (2018a) A new hybrid coupled model of atmosphere, ocean physics, and ocean biogeochemistry to represent biogeophysical feedback effects in the tropical Pacific. J Adv Model Earth Syst 10:1901–1923. https://doi.org/10.1029/2017MS001250

Zhang R-H, Tian F, Wang X (2018b) Ocean chlorophyll-induced heating feedbacks on ENSO in a coupled ocean physics–biology model forced by prescribed wind anomalies. J Clim 31:1811–1832. https://doi.org/10.1175/JCLI-D-17-0505.1

Zhang R-H, Tian F, Busalacchi AJ, Wang X (2019) Freshwater flux and ocean chlorophyll produce nonlinear feedbacks in the tropical Pacific. J Clim 32:2037–2055. https://doi.org/10.1175/JCLI-D-18-0430.1

Zhi H, Zhang R-H, Lin P, Wang L (2015) Quantitative analysis of the feedback induced by the freshwater flux in the tropical Pacific using CMIP5. Adv Atmos Sci 32:1341–1353. https://doi.org/10.1007/s00376-015-5064-0

Zhi H, Zhang R-H, Lin P, Yu P (2019) Interannual salinity variability in the tropical Pacific in CMIP5 simulations. Adv Atmos Sci 36:378–396. https://doi.org/10.1007/s00376-018-7309-1